Correlating trace element compositions, petrology, and Raman spectroscopy data in the ~3.46 Ga Apex chert, Pilbara Craton, Australia

Joti Rouillard, Martin van Kranendonk, Stefan Lalonde, Jian Gong, Mark van Zuilen

Precambrian Research 366 (2021) 106415

Contents lists available at ScienceDirect

Precambrian Research

journal homepage: www.elsevier.com/locate/precamres

Correlating trace element compositions, petrology, and Raman spectroscopy data in the ~3.46 Ga Apex chert, Pilbara Craton, Australia

Joti Rouillard [d,*], Martin J. Van Kranendonk [a], Stefan Lalonde [b], Jian Gong [c], Mark A. van Zuilen [d]

[a] School of Biological, Earth and Environmental Sciences, University of New South Wales, Kensington, Australia
[b] CNRS-UMR6538, Laboratoire Géosciences Océan, European Institute for Marine Studies, Plouzané, France
[c] Department of Earth, Atmospheric and Planetary Sciences, Massachussets Institute of Technology, Cambridge, USA
[d] Université de Paris, Institut de Physique du Globe de Paris, CNRS, F-75005 Paris, France

ARTICLE INFO

Keywords:
Hydrothermal processes
Archean cherts
Rare Earth Elements Geochemistry
Raman spectroscopy
Micropaleontology

ABSTRACT

The Apex chert unit (~3.46 Ga, Pilbara Craton, Australia) constitutes one of the oldest sedimentary units on Earth in which putative carbonaceous microfossils have been reported. The source of carbonaceous matter (CM) in this unit, however, is hotly debated. Hydrothermal fluids have circulated through the underlying crust and up into the bedded unit; these fluids could have remobilized sedimentary microbial biomass, generated abiological hydrocarbons, or harbored in situ chemolithoautotrophic microbial communities. Are there parts of the unit where microfossils might be best preserved? A potential fossil microbiota – if present – would probably be best preserved in the stratiform portion of the unit where hydrothermal influence seems to have been lowest. In order to shed light on the history of hydrothermal overprinting and the source of carbonaceous fractions in the Apex chert, we correlate here at a high spatial resolution petrographic observations and trace element analyses over a transect from the dyke where putative microfossils were found to the stratiform part where remnants of microbial mats were found. The layered, stratiform part of the unit has positive La anomalies up to 1.7, and Light Rare Earth Element depletions, indicating a seawater source. However, as far as 300 m from the dyke, the stratiform part also shows hydrothermal brecciation, high Eu anomalies (2–12; $\mu = 4.2$) and chondritic Y/Ho ratios (24.3–30.3; $\mu = 27.0$), indicating that hydrothermal fluids have laterally infiltrated over large distances. Overall, the pervasive influence of hydrothermal fluids throughout the entire unit and the presence of carbonaceous matter both in the sedimentary part and the hydrothermal dyke is consistent with a 'hydrothermal pump' model that was earlier proposed for the nearby Dresser Formation. In this model, organic matter from surface environments is circulated along with hydrothermal fluids and redistributed in the crust and overlying sediments, therefore complicating paleobiological interpretations. Raman measurements show that most of the CM experienced temperatures of ~350 °C, while some samples contain CM with a variable, but markedly lower maturity (temperature ranging from 200 to 350 °C). Correlation to texture points out a potential mixing of pre-metamorphic CM with post-metamorphic CM during late hydrothermal events.

1. Introduction

The ~ 3.46 Ga Apex chert has been the subject of significant scientific interest since it was claimed to contain carbonaceous microfossils of a filamentous microbiota representing the oldest cellular traces of life on Earth (Schopf and Packer, 1987; Schopf, 1993). The carbonaceous microfossil-like objects of the Apex chert were initially reported to occur within sand grains of a bedded sedimentary layer (Schopf and Packer, 1987; Schopf, 1993). Sedimentary cherts, in general, are known to effectively preserve microbial assemblages and microbial mats (Alleon et al., 2018, 2016; Barghoorn and Tyler, 1965; Hickman-Lewis et al., 2018; Noffke et al., 2013; Oehler, 1976; Preston and Genge, 2010; Sugitani et al., 2009, 2006; Tice and Lowe, 2006; Trower and Lowe, 2016; Westall et al., 2011). The Apex chert microstructures were compared morphologically to modern-day cyanobacteria and interpreted as an indicator for the very early development of oxygenic photosynthesis

* Corresponding author.
E-mail address: joti.rouillard@gmail.com (J. Rouillard).

https://doi.org/10.1016/j.precamres.2021.106415
Received 5 May 2021; Received in revised form 19 September 2021; Accepted 21 September 2021
Available online 22 October 2021

on Earth. In later studies, however, it was shown that these microstructures were derived from a sample collected 50 m below the paleosurface in an intrusive hydrothermal dyke that terminates in the bedded part of the Apex chert (Brasier et al., 2002, 2005; Van Kranendonk, 2006). Since it is highly unlikely that cyanobacteria lived in such a hydrothermal subseafloor setting, a more plausible alternative was proposed by Schopf, 2007 and Schopf et al., 2018 of a community of chemolithoautotrophic organisms thriving near a hydrothermal source (see eg. Brazelton et al., 2006; Jannasch, 1985; Nakagawa et al., 2005; Wang et al., 2009).

More important, however, was the subsequent debate surrounding the biogenicity of the reported microfossils, reviewed in detail in Wacey et al. (2015). Brasier et al. (2002), Brasier et al. (2005), Brasier et al. (2011) pointed out a variety of features that are incompatible with microfossils, including the fact that they occur both inside and outside of sand grains, and that their ultrastructure is filled, not hollow, as expected for bona fide microfossils. Brasier et al. (2002), Brasier et al. (2005) proposed an alternative explanation of formation. When seawater-derived hydrothermal fluids circulate through the seafloor, serpentinization of ultramafic rocks generates hydrogen and causes Fischer-Tropsch type synthesis of hydrocarbons (McCollom and Seewald, 2006; Milesi et al., 2015). Since Archean seawater was enriched in silica (Siever, 1992; Konhauser, 2007), circulating hydrothermal fluids would concentrate silica at high temperature and cause its rapid polymerization when reaching the seafloor and mixing with cooler seawater. Based on this Archean hydrothermal setting, Brasier et al. (2002), Brasier et al. (2005) reinterpreted the carbonaceous microstructures as abiotic artifacts produced by the accumulation of hydrocarbons – produced by Fischer-Tropsch type synthesis - on the edges of crystallizing siliceous spherulites.

Triggered by this controversy, numerous studies on the Apex chert followed, arguing for or against a biological origin. Arguments in favor of a biological origin were presented by Schopf & Kudryavtsev, 2009, who reported potential traces of microbial ultrastructure, including segmentation. De Gregorio et al., (2010) identified aromatic domains and oxygenated functional groups, similar to those found in well-described carbonaceous microfossils in the 1.88 Ga Gunflint Formation. Schopf et al. (2018) also presented texture-specific carbon isotope compositions, in line with specific methane-metabolizing autotrophic microorganisms. In contrast, García-Ruiz et al. (2003) demonstrated that self-organizing crystalline aggregates (silica-witherite biomorphs) synthesized experimentally may display a wide variety of life-like morphologies, including filaments similar to the Apex chert microstructures. Filamentous biomorphs could have been synthesized in Archean hydrothermal environments (García-Ruiz et al., 2020; Rouillard et al., 2018) and may have adsorbed organic matter (García-Ruiz et al., 2003), thus resulting in objects very similar to the Apex chert microstructures. Marshall et al. (2011) and Pinti et al. (2009) interpreted the filamentous microstructures to be aggregates of hematite microcrystals, although it must be noted that they were observing a population of structures distinct from the one initially reported by Schopf (1993). Wacey et al. (2015) used scanning and transmission electron microscopy to interpret the microstructures as exfoliated phyllosilicates coated by a carbonaceous material. Bower et al. (2016) used the orientation of quartz crystals in the surrounding matrix, and 3-D analysis of thin section volumes, to show that some microstructures from the original study (namely '*Eoleptonema apex*') were post-recrystallization fractures filled with carbonaceous matter, also raising caution on the biogenicity of the other originally reported structures.

Thus, as a training ground for testing cutting-edge analytical techniques and for discussing biogenicity, the Apex chert has contributed greatly to the development of the fields of life detection and Archean micropaleontology, in general. More recently, micropaleontological interest in the Apex chert was renewed by the finding of organo-sedimentary structures, potentially indicative of microbial activity, in the bedded Apex chert (Hickman-Lewis et al., 2016). This raises a critical question as to whether depositional environments and carbonaceous material are fundamentally different between the stratiform bedded chert and the hydrothermal dyke. A second critical question is whether there are parts of the unit where microfossils might be best preserved, and notably, whether there are parts that are less affected by hydrothermal alteration.

Previous investigations of the Apex chert and associated hydrothermal dykes reported textural evidence for a decrease in hydrothermal activity away from the dyke opening (Brasier et al., 2002, 2005, 2011; Van Kranendonk, 2006). It could thus be expected that a potential fossil microbiota – if present - would be best preserved in the bedded part of the unit where hydrothermal influence was minimal. However, to our knowledge, there has been no systematic study of the bedded and intrusive components of the Apex chert to test this hypothesis. While Rare Earth Element (REE) data have been reported from other parts of the Apex chert (Kato and Nakamura, 2003), they have never been used to interpret depositional environments in this specific locality. Raman spectroscopic analyses, which have indicated in previous studies the potential presence of several pools of carbonaceous matter in the Apex chert, are limited to a few samples (Brasier et al., 2002; Marshall et al., 2011; Olcott Marshall et al., 2014; Schopf et al., 2002; Sforna et al., 2014). Measurements from a larger number of samples, coming from various places, are needed to test whether carbonaceous material in the bedded Apex chert is less altered by hydrothermal activity and/or represents a distinct pool from the material in the hydrothermal dyke.

Here, we present the results of a systematic study of a transect through the main hydrothermal dyke that has been the subject of previous studies, into the stratiform part of the Apex chert. Along this transect, we report the petrography, whole-rock trace element and REE composition, and in situ Raman microspectroscopy analyses of carbonaceous material. Based on these results, we discuss whether some sections of the Apex chert represent promising targets for paleontological exploration.

2. Geologic setting

The c. 3.46 Ga Apex Basalt is part of the Warrawoona Group, in the Pilbara Supergroup, one of the oldest, best-preserved volcano-sedimentary successions on Earth, located in the Pilbara Craton of Western Australia (Fig. S1, from Brasier et al., 2011). The 3515–3423 Ma Warrawoona Group is predominantly composed of basaltic and felsic volcanic rocks, with minor intercalations of bedded sedimentary rocks (Fig. S2, from Van Kranendonk et al., 2007). The Apex chert – originally defined by Hickman (1977) – is a laterally discontinuous sedimentary unit in the Apex Basalt, and is underlain and overlain by variably altered pillow basalts (Van Kranendonk and Pirajno, 2004). It represents an extensively silicified seafloor sediment; traces of bedding and cross-bedding in even the most heavily silicified parts clearly indicate a clastic origin for this unit, which can be traced along strike for several kilometers (e.g., Van Kranendonk, 2006). Underlying the Apex chert are dense swarms of black chert hydrothermal dykes that penetrate down to 700 m below the unit and intrude up into the base of the bedded Apex chert (Brasier et al., 2005, 2011; Van Kranendonk, 2006). The Pilbara Supergroup, which includes the Apex chert, was deposited during the formation of a thick volcanic plateau. Basalts overlying and underlying the unit contain assemblages of chlorite and epidote, indicating that it has experienced low grade metamorphism (greenschist facies - Van Kranendonk et al., 2007).

The samples were collected at the southern extremity of the north block of the Apex chert, as defined by Brasier et al. (2005), during a field campaign conducted in July 2016 (Fig. 1). In this area, a large dyke (shown in black in Fig. 1), within which the debated microstructures were found (Schopf and Packer, 1987; Schopf, 1993; Schopf et al., 2002), cuts obliquely upward through underlying pillow basalts and intersects the stratiform part of the unit (shown in grey in Fig. 1). In total, 64 samples, representing a variety of bedded and/or intrusive lithologies, were collected from along the dyke and up into, and along the

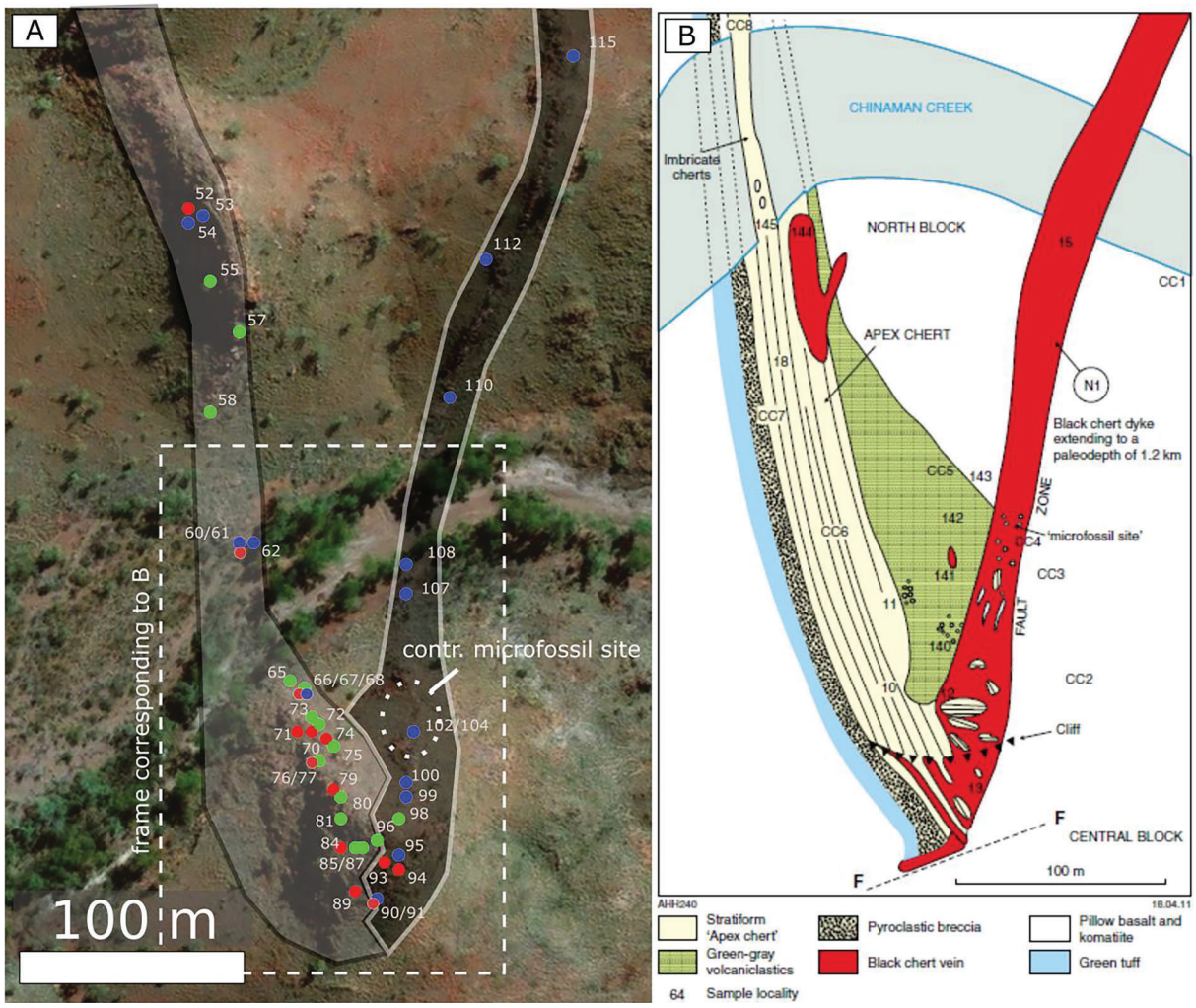

Fig. 1. Geographic and geologic provenances of the samples used in this study. **A**: Google Earth satellite view of the Apex Chert unit with GPS coordinates of the different samples overlain. The area overlain in grey represents the stratiform part of the unit. The area overlain in black represents the feeder dyke. Red dots indicate samples of purely layered chert samples, blue dots indicate samples of vein chert and green dots indicate samples presenting the two types of cherts associated (heavily veined or brecciated samples). The area inside the white, dashed frame corresponds to the area shown in B. The area inside the white, dashed circle corresponds to the controversial fossil site. **B**: Geological map from Brasier et al., 2011 (Image courtesy of the Geological Survey and Resource Strategy, Department of Mines, Industry Regulation and Safety. © State of Western Australia 2021.).

strike of, the bedded Apex chert. The location of samples analyzed during the current study is shown as dots in Fig. 1. Samples 102–105 were collected from the locality where the much-debated microfossils were first found (J.W. Schopf, pers. comm. to M.V.K, 1998).

3. Methods

3.1. Optical microscopy

Observations by optical microscopy were realized on 70 μm thick petrographic sections of the samples, using two different petrographic microscopes: a Zeiss Axio Imager A.2 m and a Leica DM 2500P (Institut de Physique du Globe de Paris - IPGP). Images were taken in transmission mode, using either plane polarized or cross polarized light.

3.2. Elemental analysis

A total of 32 sample powders (about 150 mg each) were obtained from selected sample cuts showing minimal weathering features. Powders were analyzed at the Institut Universitaire Européen de la Mer (IUEM, Brest). All weighing and digestion of sample powders for solution mode ICP-MS was carried out in a class 1000 clean lab at IUEM using PFA-distilled acids. PFA vials were acid washed internally and externally overnight in near-boiling, concentrated nitric acid (HNO_3), rinsed three times with 18.2 MW-cm ultrapure water, then dried at air temperature and stored under clean conditions. Powders were completely digested with a three-step, heated HF-HNO_3-HCl attack, with kerogen as the only residue. Approximately 100–150 mg of powder was placed in an acid cleaned PFA vial. 1.5 mL of 16 M HNO_3^- and 1.5 mL of 22 M hydrofluoric acid (HF) were added. Samples were then capped and left to react overnight at 80 °C. Samples were then uncapped and left to evaporate to dryness for 24 h. Next, 3 mL of freshly mixed *aqua regia* was added to each residue, samples were lightly capped and allowed to react for 6 h at room temperature to avoid excessive gas buildup. After 6 h, caps were removed, and the sample was evaporated overnight at 80 °C to dryness. Finally, 3 mL of 6 M HCl was added to each residue and samples were heated ~ 24 h at 80 °C. Prior to analysis, 100 μL of each sample was diluted to 5 mL with 2% HNO_3, and 1.5 mL of each sample was archived. International geostandards IF-G, BCR-2, and BHVO-2 were prepared in duplicate in the same batch and treated as unknowns to monitor precision.

Diluted samples were measured in solution mode on a Thermo Element2 HR-ICP-MS at the Pôle Spectrométrie Océan at IUEM in Brest, France. The data were calibrated against gravimetrically-prepared multi-

element standards at concentrations of 0.5, 5, and 50 ppb that were measured repeatedly throughout the session. All three multi-element solutions were measured at the beginning, end, and twice in the middle of the sequence (at 1/4 and 3/4 of the total sequence length), and the 5 ppb standard was further repeated after every five samples throughout the sequence. Additionally, 5 ppb In (Indium) was added directly to the 2% HNO3 diluant employed to prepare all solutions and was used to monitor signal stability and correct for instrumental drift across the session. Each sample and standard were bracketed by a rinse composed of the same diluant (2% HNO3 with 5 ppb) for which data was also acquired to determine the method detection limit. The international geostandards digested in the same batch (IF-G, BCR-2, and BHVO-2, see above) were included in the series as unknowns to validate the calibration achieved using multi-element solutions, yielding values generally with 5–10% of GeoREM accepted values (http://georem.mpch-mainz.gwdg.de; see Table S0 in supplementary material).

The concentrations of the different Rare Earth Elements were normalized to the concentrations in the Post-Archean Australian Shale (see line PAAS in Table S1). Several parameters were calculated:

1) Enrichment of Light Rare Earth Elements (LREE) compared to Heavy Rare Earth Elements (HREE), computed as $\frac{Pr_{PAAS}}{Yb_{PAAS}}$
2) Enrichment of Light Rare Earth Elements (Light REE) compared to Medium Rare Earth Elements (Medium REE), computed as $\frac{Pr_{PAAS}}{Sm_{PAAS}}$
3) Cerium anomaly, computed as $Ce/Ce^* = \frac{Ce_{PAAS}}{2Pr_{PAAS}-Nd_{PAAS}}$
4) Europium anomaly, computed as $Eu/Eu^* = \frac{Eu_{PAAS}}{2/3Sm_{PAAS}+1/3Tb_{PAAS}}$
5) Lanthanum anomaly, computed as $La/La^* = \frac{La_{PAAS}}{3Pr_{PAAS}-2Nd_{PAAS}}$
6) Yttrium anomaly, computed as $Y/Y^* = \frac{Y_{PAAS}}{0.5Dy_{PAAS}+0.5Ho_{PAAS}}$
7) Y/Ho ratio (Bau and Dulski, 1996).

Detection of Ce and La anomalies in the rock record must take into account the potential artifact effect of neighboring La (respectively Ce) anomalies. In order to avoid this artifact, Ce and La anomalies were calculated here using the concentrations of Pr and Nd (Bolhar et al., 2004).

Independent two-sample Student's T tests (assuming equal variance) were run using a python function (scipy.stats.ttest_ind).

3.3. Raman spectroscopy

Raman analyses were performed using a Renishaw InVia Raman microscope coupled to an Olympus BX61 Confocal microscope, within the PARI analytical platform at the IPGP in Paris. Measurements were made with a 514 nm-excitation laser (Ar-ion laser) adjusted to an on-sample intensity of 0.2 mW and a spot size of < 2 μm (50x objective). Beam centering and Raman spectral calibration were performed on a pure silicon chip with a specific Raman band at 520.4 cm^{-1}. All spectra were detected using 1800 l/mm grating, and a detector configuration in Streamspot mode, providing a spectral range of 2000 cm^{-1} in static mode. Individual spot analyses were obtained in both static mode (2 × 20 s exposure, centered at 1150 cm^{-1} with a spectral range of 100–2000 cm^{-1}) and extended mode (1 × 20 s exposure, spectral range 100–4000 cm^{-1}). In order to determine Raman spectral indicators of the carbonaceous fractions, the individual spectra were truncated to 900–1900 cm^{-1}, and a linear background subtraction was performed, using the program Wire 2.0.

Details of the Raman spectrum of carbonaceous material have been described in Sforna et al. (2014), and a short summary is given here. Pure crystalline graphite shows a single Raman peak at 1580 cm^{-1} (G-peak) representing E_{2g} bond stretching. The presence of defects in the CM structure gives rise to "disorder" peaks at ~ 1350 cm^{-1} (D1-peak), ~1620 cm^{-1} (D2-peak), ~1500 cm^{-1} (D3-peak), and ~ 1190–1250 cm^{-1} (D4-peak). Disordered CM in rocks that have not undergone temperatures above 200 °C contains all these defect-related peaks, but in more strongly altered CM these peaks are progressively lost. Increasing degrees of carbonization and graphitization can be calculated from various indicators and ratios, depending on peak-assignment protocols. In this study a 2-peak fitting protocol was applied (D-peak and G-peak) for calculating the Raman spectral indicators D-FWHM (D-peak full width at half maximum) and ID/IG (intensity-based D/G ratio), and a 5-peak protocol (D1, D2, D3, D4, G-peaks) was applied for calculating D1-FWHM (D1-peak full width at half maximum), R1 (intensity-based D1/G ratio) and R2 (area-based D1/D1 + D2 + G ratio), ID3/ID1 (intensity-based D3/D1 ratio), and ID4/ID1 (intensity-based D4/D1 ratio).

Using D1-FWHM, the Raman-based geothermometer of Kouketsu et al. (2014) was calculated. It is important to note that all commonly used Raman-based geothermometers are calibrated with bulk organic material in mudstones, shales and metapelites representing grades of increasing regional metamorphism (Beyssac et al., 2002; Kouketsu et al., 2014; Lahfid et al., 2010), or grades of contact metamorphism (Aoya et al., 2010; Kouketsu et al., 2014). Effects other than temperature can – on a local scale – affect the structural order of CM, including variations in precursor material at relatively low temperature (Qu et al., 2015), shear stress (Bustin et al., 1995), and hydrothermal fluid-induced alteration (Olcott Marshall et al., 2014, 2014; Qu et al., 2020; Sforna et al., 2014; van Zuilen et al., 2012). For this reason it has been suggested that CM in hydrothermally-altered cherts of Archean age can be better classified in a carbonization continuum using the Raman parameters D1-FWHM and R1 (Delarue et al., 2016). In the current study we use similar parameters, but also decided to at least apply one geothermometer to our dataset, in order to test whether a temperature is obtained that fits with regional lower-greenschist-facies metamorphism.

In an earlier Raman-based study of the Apex chert, Sforna et al. (2014) used the RA1-based geothermometer of Lahfid et al. (2010) for the stratiform part of the unit, and the R2-based geothermometer of Beyssac et al. (2002) for the chert vein. This was done because a significant difference in CM structural order was found between the two chert types. In our current study, in which more detail on hydrothermal fluid infiltration into the bedded parts of the chert are given, we decided to apply the D1-FWHM-based geothermometer of Kouketsu et al. (2014) that covers a continuum particularly over the temperature-range of 150–400 °C. Finally, it is important to note that Raman spectroscopy cannot be used to distinguish between a biogenic and abiogenic origin of carbonaceous materials (Pasteris and Wopenka, 2003).

4. Results

4.1. Geologic context and petrology

During this study of the Apex chert unit, the samples were separated into three types, which correspond to the three colors in Fig. 1 and Figs. 7 to 10 and which we describe in the following paragraphs:

Layered chert (red symbols in figures in Fig. 1 and Figs. 7 to 10) - The stratiform part of the Apex chert unit (shown in grey in Fig. 1) is constituted partly of layered chert. Layering consists of alternations of black/white, black/grey and/or black/red chert, oriented parallel to the bedding defined by relict clastic sedimentary textures (Fig. 2-A). This type of chert was separated by Brasier et al. (2005), Brasier et al. (2011) into three types: silicified volcaniclastics, jaspilitic cherts, and banded black-and-white cherts. They are collectively referred to here as "layered cherts". In thin section, certain layers are found to contain rounded siliceous class with sizes ranging from tens to hundreds of micrometers (Fig. 3 -B,E,F), or angular volcanic shards (Fig. 3-C). Some rare layers also display fine, wavy anisopachous carbonaceous laminations that may also drape preexisting material (Fig. 3-A,D; see Hickman-Lewis et al., 2016).

Vein chert (blue symbols in Fig. 1 and Figs. 7 to 10) - The meter-wide, hectometer-long hydrothermal dyke is constituted of massive, black to light grey chert. This intrusive chert extends as hydrothermal sills all along the stratiform part of the unit (e.g. Fig. 2-B). It lacks

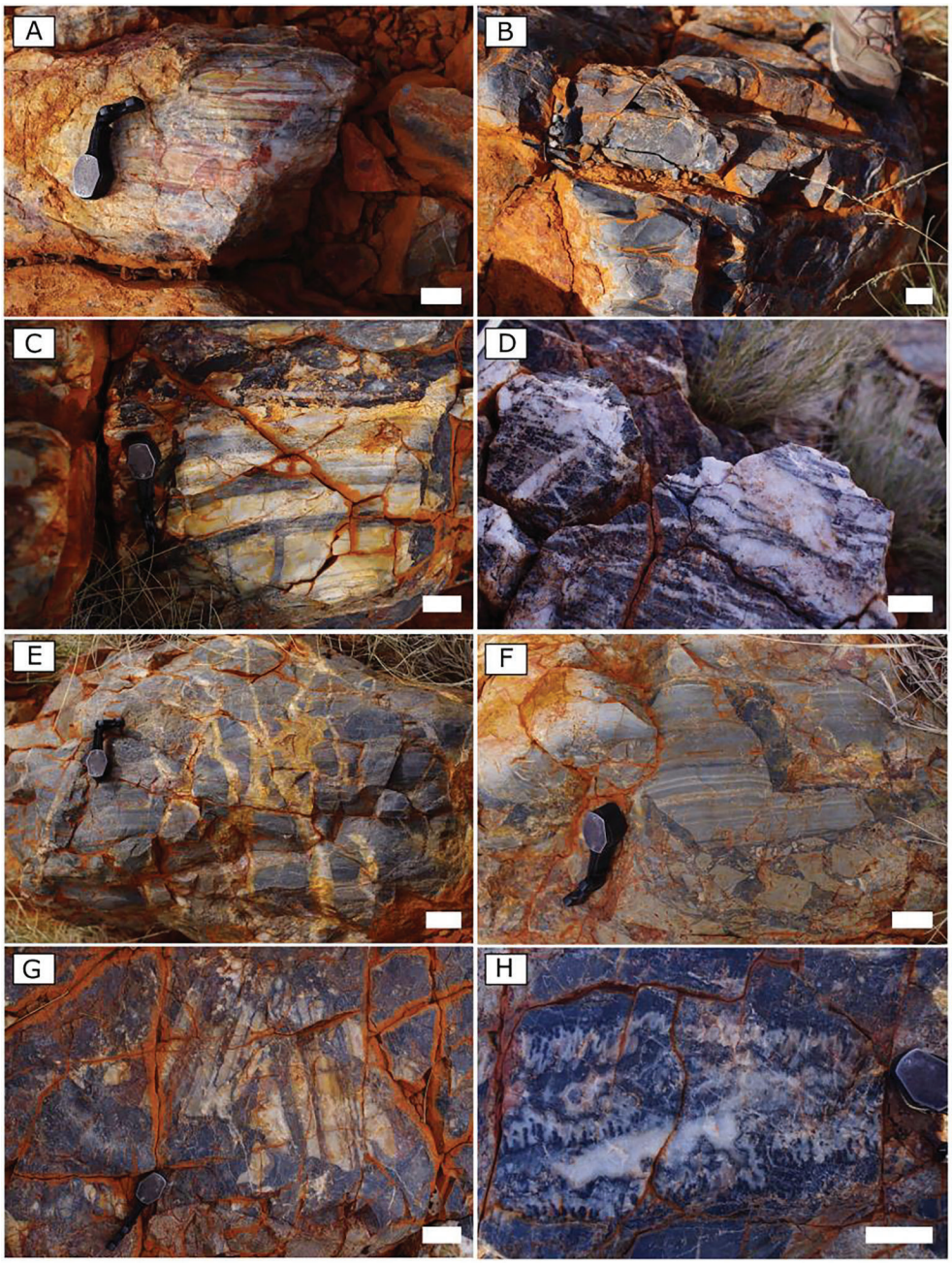

Fig. 2. Field observations of different rock facies in the Apex Chert unit. **A**: Layered chert (white/grey alternation with red surface hematitic alteration). **B**: Pure vein chert (massive dark grey sill). **C** to **G**: strongly veined to brecciated cherts. **C**: black veins running parallel to the bedding, with local cross-cutting of the white sedimentary chert by secondary veins. **D**: subhorizontal anastomosed white veins and recrystallization patches. **E**: In place brecciation of the laminated country rock. **F**: In place brecciation of the laminated country rock by dark veins (top) and movement of angular clasts (bottom). **G**: Displacement of large laminated clasts of the country rock (two different directions of lamination) by the brecciating fluid. **H**: Void-filling texture (silica botryoids). Scalebars: 3 cm.

layering or other textures indicative of sedimentary processes and displays characteristic marginal alteration haloes. Outcrop and thin section petrography of samples from the dyke reveal several generations of crosscutting and/or brecciated silica, ranging from earliest black to latest light grey chert (Fig. 4-G; see also Van Kranendonk, 2006). Breccia fragments vary from angular to subrounded.

Chert breccia (green symbols in Fig. 1 and Figs. 7 to 10) - Along the stratiform Apex chert, the layered cherts are crosscut by the intrusive chert at a centimeter to decimeter scale. This results in heavily veined (Fig. 2-C,D) to brecciated (Fig. 2-E,F) cherts. In thin section, smaller veins consist mainly of mesocrystalline quartz (crystal size range 10–100 μm) that contrasts sharply with the microcrystalline quartz in the surrounding matrix, where the crystal size ranges from 1 to 10 μm. Some veins also contain carbonaceous material, sulfides, and dispersed barite. In thin section, the matrix appears patchy, due to local differences in organic content and/or heterogeneous recrystallization (Fig. 4-B,C). In the most strongly recrystallized areas, the initial textures leave only "ghosts" (clasts in Fig. 4-B) or they even disappear completely (carbonaceous laminae in Fig. 4-C). Although it is not systematic and may depend on the timing of emplacement, the rock material also appears clearer close to certain veins, indicating a decreased concentration, or absence, of carbonaceous material (Fig. 4-A). The bedded chert is broken apart and disorganized by the veins in some samples, resulting in a mixed brecciated texture (Fig. 2-E,F,G, Fig. 4-D, E, F). The chert matrix of these breccias may be dark (Fig. 2-F,G, Fig. 4-F) or clear (Fig. 2-E, Fig. 4-D, E), depending on their crystallinity and their carbonaceous material content. Smaller pieces of the primary layered chert are sometimes moved as angular clasts and float along in the matrix (Fig. 2-F,G, Fig. 4-F).

Apart from these three lithological types, some specific features were recognized that occur among the chert samples:

Botryoidal textures - In several samples collected along the outcrop,

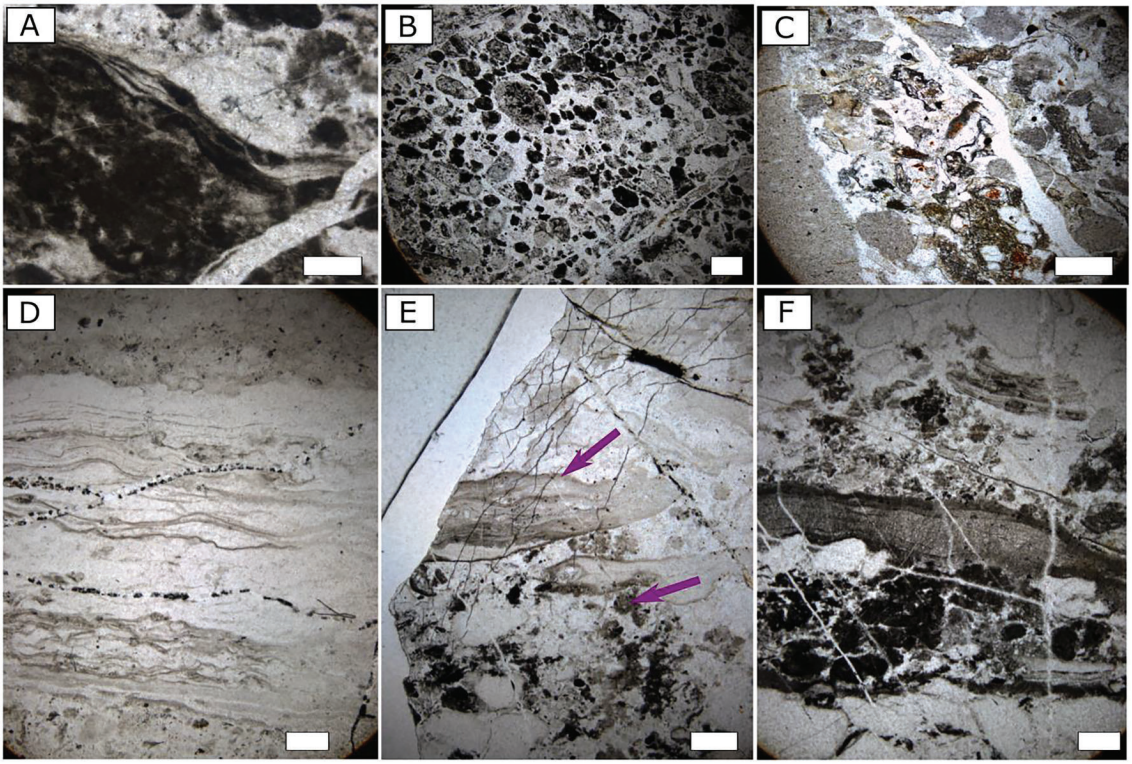

Fig. 3. Observations in petrographic thin sections of sedimentary features in some collected samples. See Fig. 1 for the geologic location of the samples mentioned. **A**: Carbonaceous drapings of carbon-rich clasts – sample #58. **B**: Silicified sandstone with well-rounded, polymict clasts. Some of the clasts represent silicified basaltic fragments. Note the diversity of carbonaceous content (diversity of opacity) between clasts – sample #58. **C**: Angular volcanic shards in a silicified sandstone bed – sample #77. **D**: Fine, wavy, anisopachous carbonaceous laminations – sample #52. **E**: Clastic layer containing large, elongated, undulating clasts with internal carbonaceous laminations –sample #65. The two arrows indicate the specific types of textures (carbonaceous laminations and organic-rich clasts) where Raman spectra were acquired (cf. §4.3). **F**: Alternating clastic and laminated layers– sample #65. One of the clasts (top right) displays carbonaceous laminations and soft deformation features. Pictures taken with an optical microscope in plain polarized light. Scalebars: 200 μm.

decimeter-size voids are filled by botryoidal growth patterns of silica - Fig. 2-H. In thin section, two main textures associated with two growth stages can be distinguished – (Fig. 5-A, B, C; see also Brasier et al., 2011). The initial stage consists of the growth of botryoidal fibrous chalcedony. This texture is layered, indicating the existence of cyclic changes in crystal size (and therefore of the nucleation rate) of quartz. The later stage consists in the growth of mesocrystalline quartz in the remaining interstitial space. The path of circulation of the fluids may change between the two stages (e.g., mesocrystalline quartz crosscutting the chalcedony botryoids in Fig. 5-A). In rare instances, opaque crystals (sulfides) are also observed lining silica botryoids (Fig. 5-C). Carbonaceous botryoids, i.e carbon-bearing laminae separated by isopachous silica layers, were also identified in three samples (# 61, 107, 108; Fig. 5-D). The texture of the silica associated with these botryoids does not differ from the texture of the silica in the rock matrix. Botryoidal void fills are characteristic of epithermal environments, including that of the slightly older Dresser Formation in the Pilbara Supergroup (e.g. Harris et al., 2009; Van Kranendonk and Pirajno, 2004). Since botryoidal textures represent a secondary void-filling growth pattern, the organic matter associated with them either i) was leached and remobilized from the surrounding rock or ii) originated from the hydrothermal fluid precipitating as botryoids. In either case, these organic-rich growth laminae were emplaced during a later-stage hydrothermal event, and are therefore considered secondary.

Recent weathering - At the surface, the Apex chert, like other units in the Pilbara, has been affected by weathering from the Cenozoic to present (Thiry et al., 2006). Late fissures facilitate the circulation and redeposition of red/brown iron oxy-hydroxides, observable along cracks at the outcrop and in thin sections (Fig. 2, Fig. 5-E). In thin section, some mineral alteration products (clay-like phyllosilicates, potentially resulting from the alteration of feldspars in neighboring basalts) can also be locally observed (Fig. 5-F). This late weathering may explain the description of hematitic structures in the Apex chert by (Marshall et al., 2011).

4.2. Trace element geochemistry

Measured whole rock concentrations of REE, Y, Zr, Ni, and Al (all in ppm) for Apex chert samples are presented in Table S1. All REE distributions measured in the current study are shown on Fig. 6. The corresponding total REE concentrations, $(Pr/Yb)_{PAAS}$ and $(Pr/Sm)_{PAAS}$, La and Eu anomalies, Y/Ho ratios, Zr and Ni concentrations are presented in Table 1 and shown in Fig. 7 for the different chert types.

A series of Student's t tests were run in order to evaluate whether statistically significant differences exist between samples of vein cherts and layered cherts. These tests were made for $\sum REE$, $(Pr/Yb)_{PAAS}$ and $(Pr/Sm)_{PAAS}$, La and Eu anomalies, Y/Ho ratios, and Zr and Ni concentrations. Results of the tests are given in Table S2. These chert types do not show significant differences in $\sum REE$, La and Eu anomalies, Y/Ho ratios and Ni concentrations. $\sum REE$ in all Apex chert samples range between 0.26 and 19.65 ppm (average value $\mu = 6.28$ ppm, Standard deviation SD = 4.60 ppm). La/La^* range between 0.78 and 1.67 ($\mu = 1.15$, SD = 0.21). Eu/Eu^* range between 1.91 and 5.55 ($\mu = 3.83$, SD = 2.04), with 4 outliers between 7.52 and 10.32. Y anomalies do not deviate largely from 1, ranging from 0.84 to 1.10 ($\mu = 0.98$, SD = 0.07), and Y/Ho ratios are consistently chondritic; they range between 24.29 and 29.99 ($\mu = 26.95$, SD = 1.59). Ni concentrations range between 0.68 ppm and 29.17 ppm ($\mu = 12.46$ ppm, SD = 18.22 ppm), with 4 outliers between 38.35 ppm and 85.40 ppm. Vein cherts and Layered cherts, on the other hand, show significant differences for $(Pr/Yb)_{PAAS}$,

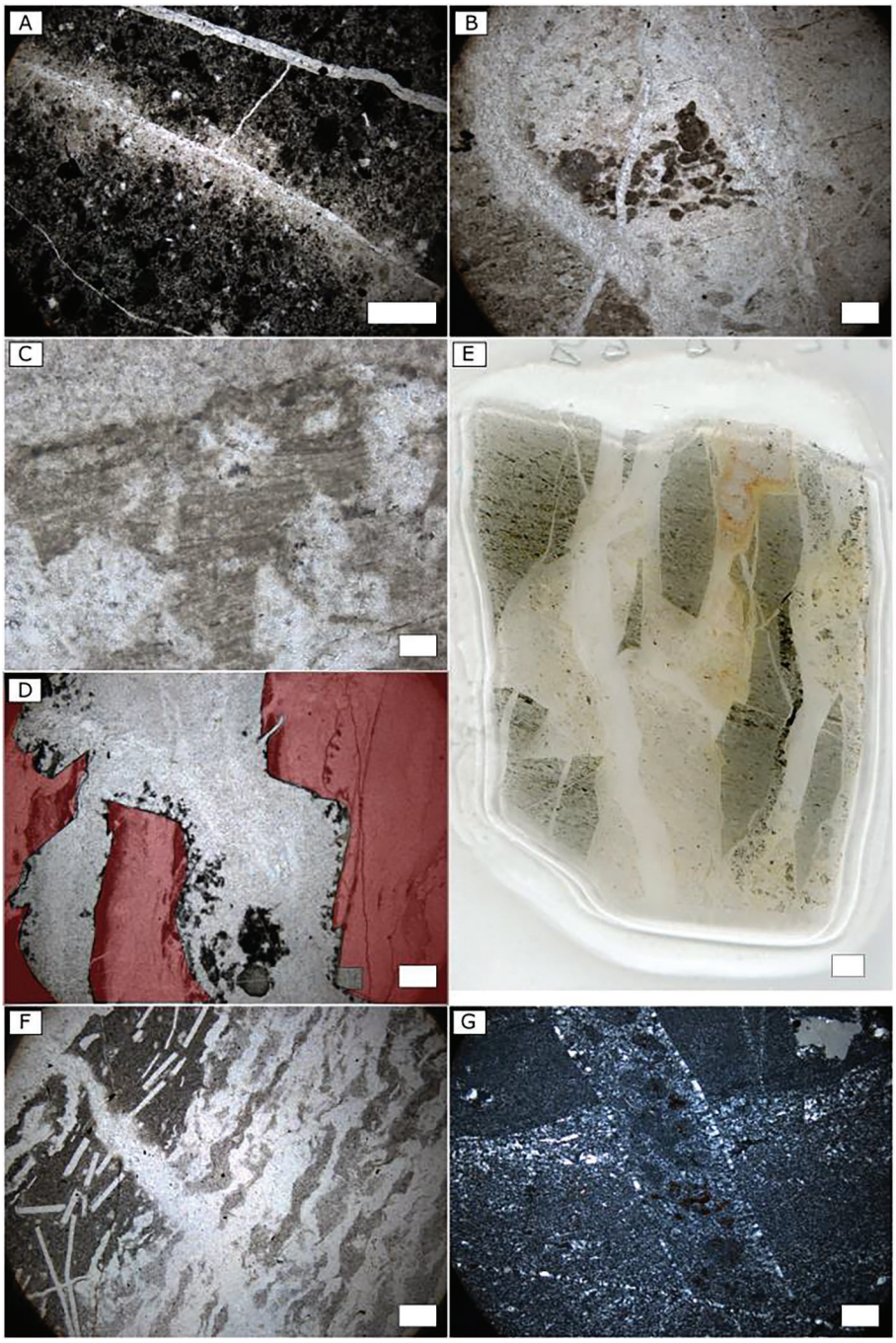

Fig. 4. Observations in petrographic thin sections of veining, recrystallization and brecciation features in some collected samples. **A**: Veins of mesocrystalline quartz cutting through a carbonaceous-rich clastic layer of the country rock – sample #62. The central vein bleaches the host rock. **B**: Loss of the texture in a recrystallizing carbonaceous-rich clastic layer; the central zone preserves the initial texture, whereas the top and bottom zones show only 'ghosts' of the clasts – sample #55. **C**: Disappearance of carbonaceous laminae in patches where silica recrystallizes – sample #55. **D**: In-place brecciation of the country rock and escape of dark carbonaceous material from the country-rock (shaded in red/brown here) to the carbonaceous-poor brecciating phase – sample #65. **E**: In-place brecciation illustrated on a thin section scan – sample #68. **F**: Angular clasts 'floating' in a dense, dark hydrothermal brecciating fluid – sample #60. **G**: Intrusive vein sample with crosscutting textures indicative of several phases of hydrothermal circulation, brecciation and recrystallization – sample #93. All pictures except E taken with an optical microscope in plain polarized light - A to D and F - or in cross-polarized light (G). Scalebars: 200 μm, except E: 2 mm.

$(Pr/Sm)_{PAAS}$ and Zr concentrations (respectively p of 0.107, 0.102 and 0.106). Layered cherts are on average more depleted in LREE than vein cherts, with average $(Pr/Yb)_{PAAS}$ of 0.74 (SD = 0.49) for layered cherts, versus 1.02 (SD = 0.46) for vein cherts. Layered cherts contain on average more Zr than vein cherts, with an average Zr concentration of 6.54 ppm (SD = 5.91 ppm) for layered cherts, and an average Zr concentration of 3.58 ppm (SD = 3.07 ppm) for vein cherts. Following Bau & Dulski (1996), only two samples, which are interpreted as outliers, displayed "true" negative Ce anomalies (Fig. S3). Given their statistical rarity, they were considered as outliers and this negative anomaly is not further discussed in this study.

4.3. Raman spectroscopy of CM

Raman measurements were made on wavy organic laminations concordant with stratigraphy found within layered cherts (see §4.1; Upper arrow in Fig. 3-E; Fig. S4, Panel I-A to C), on carbon-rich clasts found in sedimentary clastic layers (§4.1; Lower arrow in Fig. 3-E; Fig. S4, Panel I-D to F), and on widespread amorphous cloths for which an origin cannot be attributed with certainty. In addition, a number of measurement was taken specifically on the CM found within secondary botryoidal growth zones (§4.1; Arrows in Fig. 5-D; Fig. S4, Panel II).

Raman spectral characteristics of all combined CM throughout the study area display a significant range in degree of carbonization, from highly ordered to strongly disordered (Fig. 8-A; Table 2; Rouzaud et al., 2015; Delarue et al., 2016). A range of *ID1/IG* ratios of 0.83 to 1.71 and a

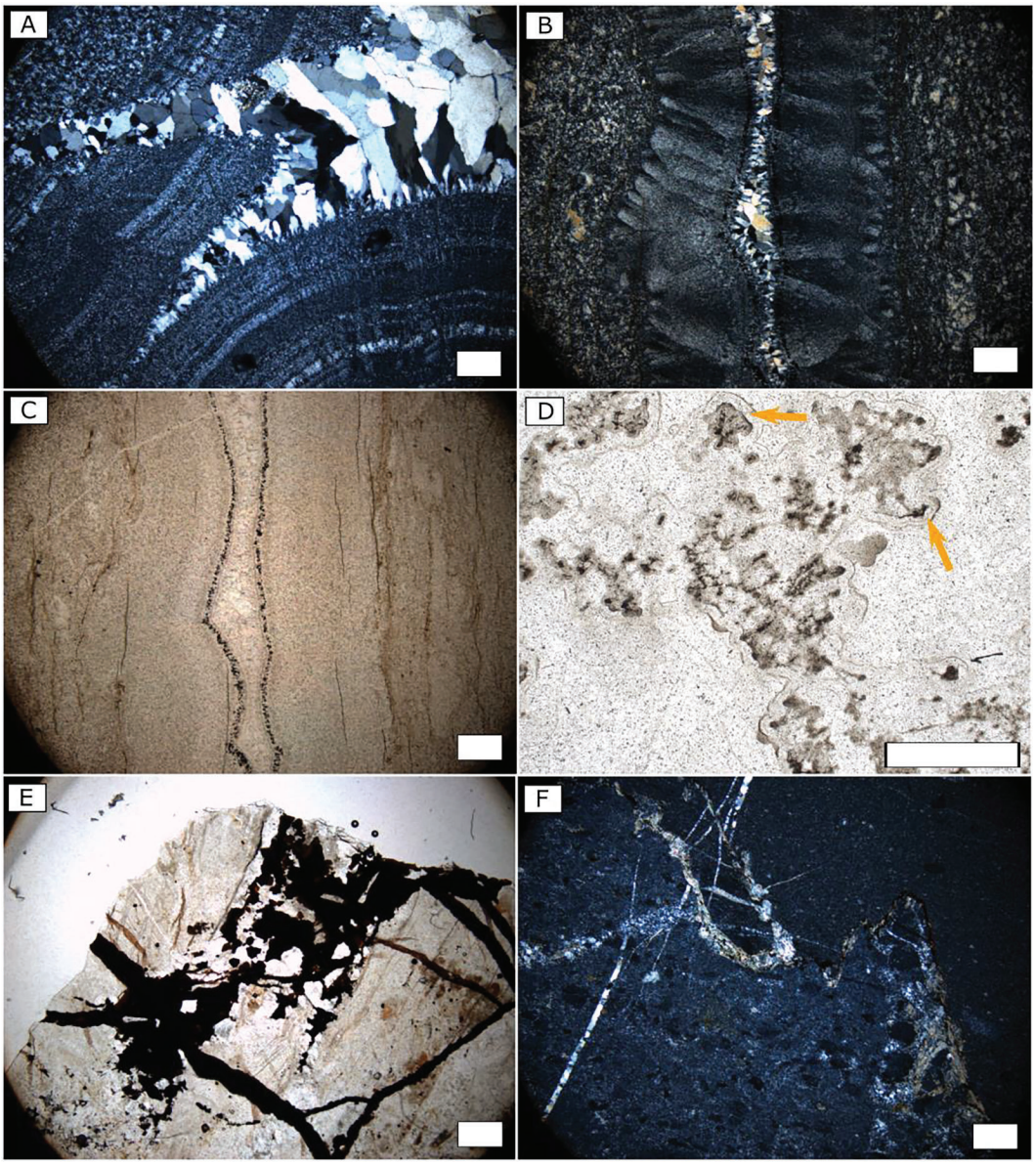

Fig. 5. Observations in petrographic thin sections of secondary features in some collected samples. **A** to **D**: Void-filling textures. **A**: Botryoid texture with early discontinuous chalcedony growth and late mesoquartz filling, crosscutting the chalcedony – sample #60. **B** and **C**: Botryoid texture with early discontinuous chalcedony growth, intermediate sulfide crystallization and late mesoquartz filling – sample #88. **D**: Carbonaceous 'flowers'– sample #107. The two arrows indicate the specific type of texture (carbon-rich botryoidal growth zones) where Raman spectra were acquired (cf. §4.3) **E**: fissures associated to Cenozoic weathering and filled by iron oxides (hematite) – sample #85. **F**: Weathered zone showing clay-like phyllosilicates – sample #77. These minerals probably derive from the alteration of feldspars in nearby basaltic rocks. All pictures taken with an optical microscope in cross polarized light - A, B, F- or in plain-polarized light - C to E. Scalebars: 100 μm, except D: 300 μm.

range of *D1-FWHM* of 51.3 to 138.7 cm^{-1} is observed (Fig. 8-B). CM in the large majority of samples display quite uniform Raman spectral shapes with D1-FWHM of 60.66 +/- 11.98 cm^{-1} and ID1/IG of 1.42 +/- 0.13, in line with the earlier study by Sforna et al., 2014 (Fig. 8-B). They correspond to peak T-D1 temperatures around 350 °C (348 +/- 26 °C; Fig. 8-C). We refer collectively hereafter to these samples as group α. Only six samples of vein cherts and chert breccia and one sample of layered chert display a particularly large range in spectral characteristics. These are found in several places along the studied outcrop, both in the stratiform part (samples of vein cherts and breccia #58, 61, 62, 65, and sample of layered chert #71) and in the hydrothermal dyke (samples #107, 108). We refer collectively hereafter to these samples as group β. In Group β samples, a range of temperatures from 252 °C to 360 °C has been calculated using the *D1w*-based geothermometer *T-D1* of Kouketsu et al. (2014) (Fig. 8-C). Interestingly, organic laminations concordant with stratigraphy found within layered chert and carbon-rich clasts in sedimentary clastic layers display high ID1/IG values and low D1-FWHM, similar to sample group α (Fig. 8-D, purple circles). In contrast, CM in void-filling botryoid textures display a range of maturities (Fig. 8-D, orange diamonds) corresponding to the ones measured in sample group β.

5. Discussion

5.1. Depositional environment of the Apex chert - insights from trace element data

Cherts may form either through direct precipitation from a silica-rich fluid (primary chert), through silica sorption and precipitation during

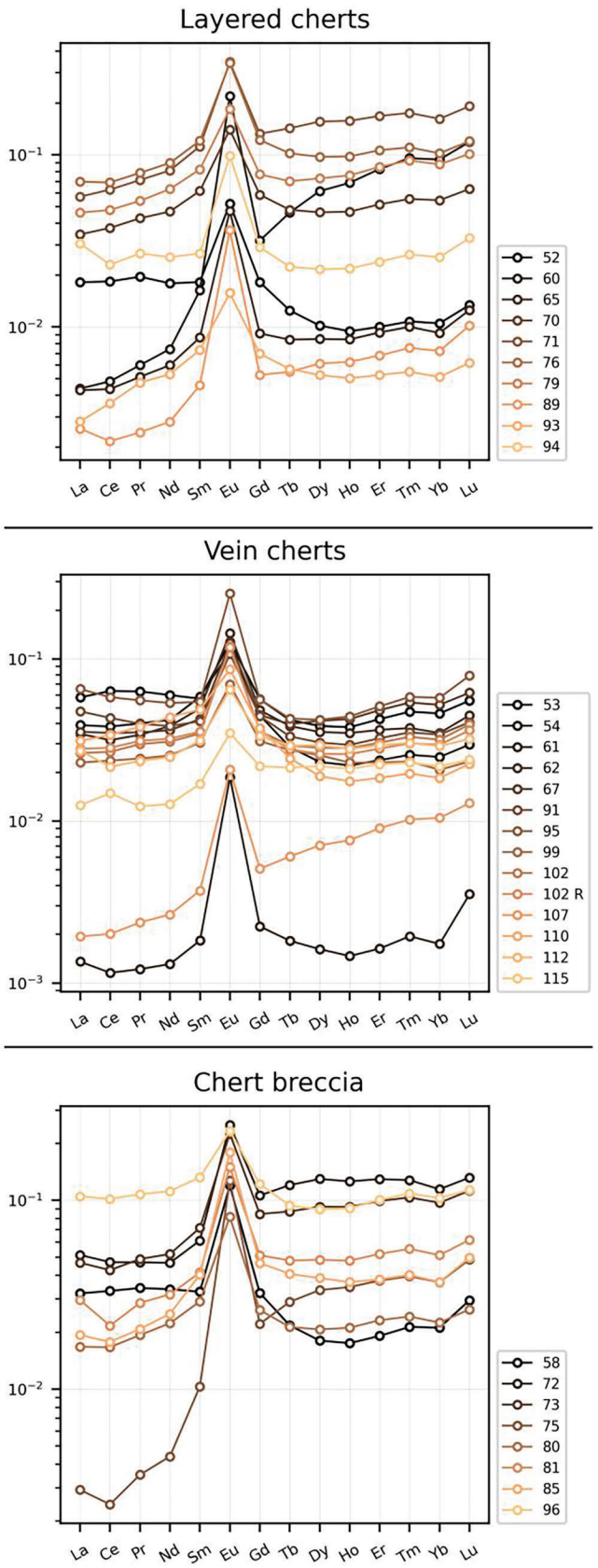

Fig. 6. REE patterns (concentrations in ppm normalized to the PAAS) measured in Apex Chert samples and grouped by type of lithology.

early diagenesis of clastic sediments (chemico-clastic cherts), or through later silicification of a pre-existing rock (secondary chert) (Ledevin et al., 2014; Rouchon and Orberger, 2008; van den Boorn et al., 2007; van den Boorn et al., 2010). The nature of silica-rich source fluids may also vary, ranging from seawater to hydrothermal fluids and other non-marine waters, such as freshwater or lagoonal water (Bau and Dulski, 1996; Bolhar and Vankranendonk, 2007; Elderfield et al., 1990; Hickman-Lewis et al., 2020; Kamber et al., 2004). The REE composition of cherts and carbonates is believed to reflect the characteristics of these source fluids and/or specific paleoenvironmental conditions:

- Marine waters are recognized in shale-normalized REE patterns by a characteristic enrichment in Heavy REE compared to Light REE, a pronounced La anomaly and superchondritic Y/Ho ratios with significantly positive Y anomalies – most marine waters exhibit Y/Ho ratios above 40 (Bau and Dulski, 1999; Nozaki et al., 1997; Sholkovitz et al., 1994). Modern oxic seawaters also exhibit Ce anomalies which are usually not found in samples derived from anoxic Archean seawaters.
- Hydrothermal fluids are recognized by strongly positive Eu anomalies (Douville et al., 2002; Mitra et al., 1994; Thurston et al., 2012). It has also been suggested that the magnitude of a Eu anomaly is indicative of hydrothermal fluid temperature (Kato and Nakamura, 2003; Wheat et al., 2002). Although these anomalies are not preserved in modern seawater due to efficient scavenging on iron oxyhydroxyde particles, lower redox potentials probably led to their persistence in Archean and Paleoproterozoic seawaters (Danielson et al., 1992; Kamber and Webb, 2001).
- Igneous phases (input of detrital particles or incomplete protolith replacement), which are richer in REE than aqueous precipitates (Condie, 1993; Rudnick, 2003), are identified by increased concentrations in REE and flat shale-normalized patterns.
- REE complexation by organic groups on cell walls can affect the REE composition (Takahashi et al., 2005) and may notably be identified by specific enrichments in the heaviest REE - Tm, Yb and Lu - in the organic phase (see conclusions in Takahashi et al. 2005), corresponding to a specific depletion in the same elements in associated precipitated inorganic phases.

Since REE compositions are highly sensitive to environmental conditions at the time of deposition and poorly sensitive to post-depositional events (such as metamorphism), they have been used to interpret the depositional setting of a number of Archean and Paleoproterozoic cherts and carbonates (e.g., Allwood et al., 2010; Bau and Dulski, 1996; Bolhar et al., 2005, 2004; Bolhar and Vankranendonk, 2007; Gourcerol et al., 2015; Hickman-Lewis et al., 2020; Kamber et al., 2004; Kamber and Webb, 2001; Kato and Nakamura, 2003; Sugahara et al., 2010; Thurston et al., 2012). The PAAS-normalized REE patterns of Apex chert samples display a strong variability (Fig. 6). The range of $(Pr/Yb)_{PAAS}$ values measured in the Apex chert is consequently larger than those reported in several Paleoproterozoic and Archean sedimentary chert units (Bau and Dulski, 1996; Gourcerol et al., 2015; Hickman-Lewis et al., 2020). It is comparable to ranges reported in the Quartzite/Cleaverville formations and in the Strelley Pool formation (Allwood et al., 2010; Sugahara et al., 2010), where paleoenvironmental conditions - and the relative influence of seawater, non-marine waters and/or hydrothermal fluids – were interpreted to vary along stratigraphy. Where does this variation in shape come from in the Apex chert unit?

The possibility that some parts of the Apex chert were formed by replacement of the basaltic/komatiitic seafloor appears unlikely, since (i) concentrations of Ni (which is enriched in mafic lithologies) are on average similar to, or lower than Ni concentrations in other chemically precipitated cherts (Fig. 7) and (ii) the Ni concentration is not correlated to REE concentrations (Fig. 9-B). On the other hand, a statistically significant positive correlation between Zr (and Th) and REE concentrations ($r = 0.7$, $p = 2e\text{-}6$; Fig. 9-C) indicates the influence of detrital input

Table 1
REE-associated parameters, Zr and Ni concentrations obtained on the different samples. Each row in the table represents measurements from a single sample powder. Measurement was repeated on two different powders for sample 102. *Petrology*: type of sample; LC: layered chert, VC: vein chert, CB: chert breccia. The position of the sample is calculated as the geographic distance (*D*, in meters) from sample #90 (representing the opening of the intruding dyke). Increasingly negative distances from sample #90 represent samples further north in the stratiform part of the unit (grey area in Fig. 1) - that is, increasing distance from the opening of the dyke. Increasingly positive distances represent samples further north in the intruding dyke (black area in Fig. 1) – that is, increasing paleodepth in the dyke. $\sum REE$ is the sum of raw REE concentrations in ppm. $(Pr/Yb)_{PAAS}$ represents the enrichment of light to heavy REE. $(Pr/Sm)_{PAAS}$ represents the enrichment of light to medium REE. *La/La**, *Eu/Eu** and *Y/Y** stand for La, Eu and Y anomalies respectively. See methods for computation of parameters.

Sample nr	Petrology	D (m)	∑REE (ppm)	(Pr/Yb)paas	(Pr/Sm)paas	La/La*	Eu/Eu*	Y/Y*	Y/Ho	Zr (ppm)	Ni (ppm)
52	LC	−284	3,31	1,87	1,07	0,80	3,23	0,87	24,68	0,80	2,62
53	VC	−280	11,13	1,37	1,11	0,83	2,48	0,94	25,76	6,47	2,47
54	VC	−279	7,30	1,61	0,68	1,09	2,32	0,95	26,54	2,24	2,05
58	CB	−208	6,03	1,62	1,05	0,91	4,16	0,94	26,04	3,64	29,17
60	LC	−157	2,31	0,06	0,37	1,41	8,45	1,00	25,86	14,29	38,35
61	VC	−157	0,26	0,70	0,67	1,31	10,32	1,03	29,49	0,24	4,44
62	VC	−156	6,57	0,97	0,69	1,38	3,18	1,02	27,92	3,71	46,82
65	LC	−102	1,02	0,56	0,59	1,26	5,55	0,97	26,54	1,62	40,97
67	VC	−98	6,87	0,68	0,83	1,07	3,04	0,99	26,73	6,42	5,96
70	LC	−81	7,69	0,79	0,69	0,99	2,48	0,97	26,22	5,85	4,11
71	LC	−83	14,26	0,44	0,64	1,10	2,86	1,10	29,77	13,26	17,63
72	CB	−83	10,43	0,41	0,77	1,07	3,12	1,08	29,79	9,28	9,73
73	CB	−87	9,65	0,50	0,68	1,09	2,97	1,02	27,78	11,11	85,40
75	CB	−74	1,25	0,10	0,34	1,67	7,74	1,02	27,33	2,89	6,73
76	LC	−70	14,82	0,77	0,65	1,24	3,01	1,10	29,99	11,65	2,90
79	LC	−58	10,25	0,61	0,66	1,30	2,39	0,95	25,30	13,09	5,34
80	CB	−55	3,55	0,86	0,66	1,26	3,11	1,03	27,84	2,07	3,23
81	CB	−47	5,47	0,56	0,69	1,32	3,48	1,00	27,50	4,66	3,78
85	CB	−35	4,32	0,56	0,52	1,56	4,48	0,95	26,67	5,49	15,57
89	LC	−19	0,56	0,34	0,53	1,51	7,52	1,10	29,64	0,34	0,74
91	VC	14	7,90	1,17	0,97	1,12	2,81	0,89	24,62	6,70	4,19
93	LC	26	0,78	0,93	0,65	0,78	2,34	0,98	27,23	0,29	0,68
94	LC	22	4,79	1,05	1,00	1,04	3,95	1,02	27,69	4,24	2,89
95	VC	28	10,91	0,96	1,02	1,10	5,07	1,05	28,10	11,34	24,09
96	CB	35	19,65	1,05	0,81	1,05	1,97	0,95	25,69	11,00	3,69
99	VC	48	4,53	1,17	0,80	1,04	2,38	0,84	24,29	0,59	1,38
102	VC	71	5,32	0,94	0,86	0,95	3,68	0,99	26,97	2,27	3,22
102 R	VC	71	5,55	1,06	0,88	0,96	3,62	1,01	27,55	2,27	3,52
107	VC	122	0,52	0,23	0,64	1,07	4,66	1,01	26,70	1,23	15,26
110	VC	189	6,52	2,07	0,78	1,16	2,15	0,88	24,83	2,13	3,03
112	VC	235	4,59	0,81	0,75	1,30	2,13	0,93	26,09	2,58	3,87
115	VC	300	2,72	0,57	0,73	1,09	1,91	0,91	25,36	2,01	4,97

of felsic origin (such as granitoids/TTGs). This detrital input may have two origins: (1) the Pilbara supergroup was deposited in an environment of a volcanic caldeira (Kato and Nakamura, 2003; Van Kranendonk et al., 2007); volcanic shards and zircon have also been observed in some samples of the Apex chert (Fig. 3-C). Detrital input can therefore be explained by infalls from felsic explosive volcanic events. (2) Similar detrital input has been reported in sedimentary cherts from the 2.7 Ga Woodburn Lake Group (Canada) and the 3.4–3.2 Ga Barberton Greenstone Belt (South Africa), where it is believed to represent discharge of continental crust weathering products into epicontinental basins (Bolhar et al., 2015; Gourcerol et al., 2015; Hickman-Lewis et al., 2020). Input from non-marine waters with a detrital load and lacking the REE signature of seawater is also consistent with the small La anomalies and chondritic Y/Ho ratios measured in the Apex chert. Irrespective of the origin of this detrital input, a negative correlation between Pr/Yb_{PAAS} and Zr concentration ($r = 0.28$, $p = 0.10$; Fig. 9-D) implies that it has a significant influence on the general shape of REE patterns in the Apex chert. The lack of correlation between Zr concentration and La/La* or Eu/Eu* (respectively p of 0.43 and 0.61 – Fig. 9-E,F), however, means that the detrital fraction does not obscure all other characteristics in the chert REE composition.

The influence of seawater can be observed in some samples by a significant depletion in Light REE and by positive La anomalies. It is further substantiated by a negative correlation between Pr/Yb_{PAAS} and Y/Ho ratios, and Pr/Yb_{PAAS} and La anomalies (Fig. 9-G,H). The Pr/Yb_{PAAS} and Pr/Sm_{PAAS} are lower in layered cherts than in vein cherts (Fig. 9-A; Table S2), which may indicate a more pronounced influence of seawater in these samples. However, no significant difference in Y/Ho and La anomalies was found between these two groups of samples (Table S2). Overall, La anomalies (0.78–1.67) and Y/Ho ratios (24.29–29.99) in the Apex chert are quite low compared to other Archean and Paleoproterozoic sedimentary cherts (Allwood et al., 2010; Bau and Dulski, 1999; Bolhar et al., 2005; Gourcerol et al., 2015; Hickman-Lewis et al., 2020; Sugahara et al., 2010), and with a range from 0.84 to 1.10, no significantly positive Y anomaly were found. Although a seawater influence can be locally recognized, it appears quite negligible at the scale of the unit. We also note that no significant negative Ce anomalies (*sensu* Bolhar (2004); see also Fig. S3) were detected here, which is in line with REE measurements in other Archean rocks and is generally interpreted as indicative of a globally anoxic Archean atmosphere/hydrosphere (Allwood et al., 2010; Arndt and Nisbet, 2012; Kamber and Webb, 2001; Van Kranendonk et al., 2003; review in Kamber et al., 2014).

Eu anomalies in the different lithological types of the Apex chert (including the layered cherts) are high, compared to other Archean and Proterozoic sedimentary cherts (e.g Allwood et al., 2010; Bau and Dulski, 1996; Hickman-Lewis et al., 2020; Sugahara et al., 2010). The observed average Eu* of 3.83 is similar to anomalies measured in samples from the Panorama formation (Bolhar et al., 2005) and the Woodburn Lake group (Gourcerol et al., 2015), where a significant influence from hydrothermal fluids was inferred. This is consistent with an active hydrothermal vent system at the time of deposition of the Apex chert. It has been found before that hydrothermal alteration of basalts releases preferentially Light REE into the solution, leading to flattened REE patterns (Van Kranendonk and Pirajno, 2004). Such a process would be represented by a positive correlation between Eu anomalies and Pr/Yb_{PAAS} which is not observed in the Apex chert (Fig. 9-I). The enrichment in light REE appears to originate from detrital inputs (negative correlation between Zr

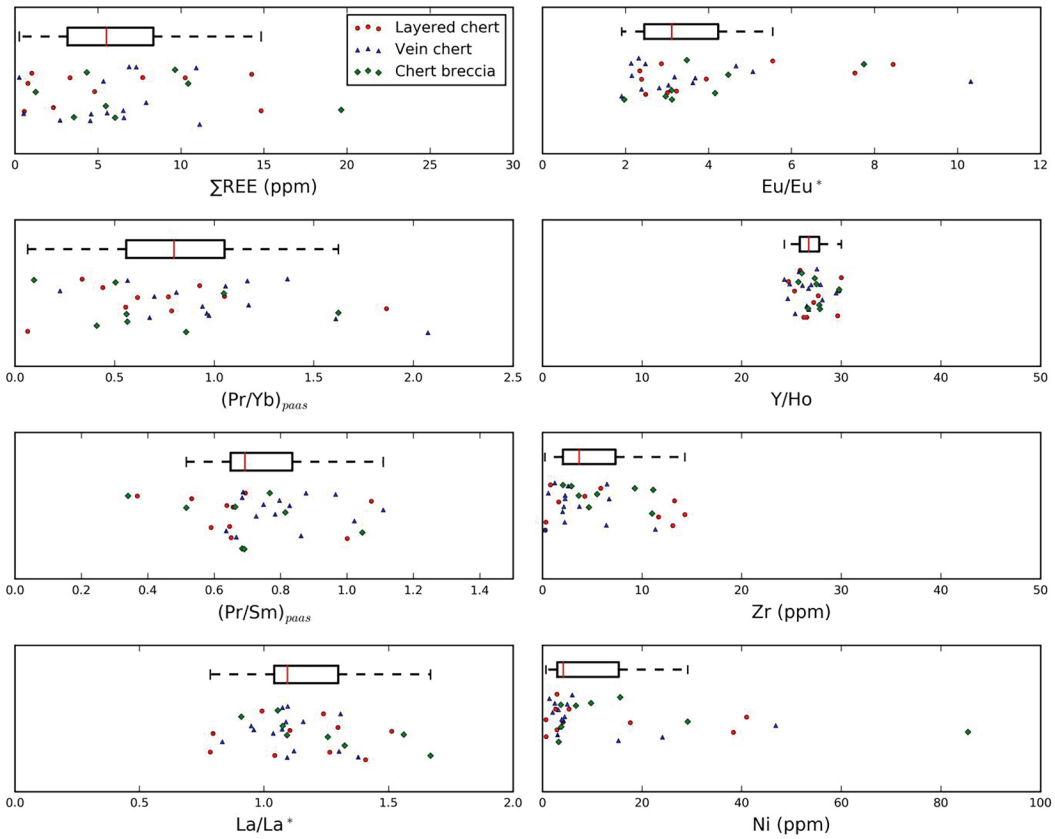

Fig. 7. REE + Y chemistry, Zr and Ni contents in Apex chert samples. The box extends from the first (Q1) to the third (Q3) quartile of the data, with the red central line corresponding to the median. Whiskers extend according to Tukey's original definition of boxplots (Tukey, 1977), and exclude as outliers data below Q1 – 1.5* (Q3-Q1) or above Q3 + 1.5(Q3-Q1).

concentration and Pr/Yb_{PAAS}, Fig. 9-D).

No specific depletion or enrichment in Tm, Yb and Lu compared to neighboring elements could be found in the PAAS-normalized REE patterns; as a consequence, the effect of REE complexation by cell walls is considered negligible in the samples studied.

In general, the REE compositions indicate that the Apex chert was precipitated chemically from anoxic waters, strongly influenced by hydrothermal fluids and detrital input – from volcanic infall or continental runoff - that obscured typical seawater signals. Changes in the intensity of hydrothermal influence and in the amount of detrital input explain the strong variations in REE composition in the unit.

5.2. *Maturity of carbonaceous materials in the Apex chert*

Previous Raman measurements in the Apex chert unit, conducted on a small number of thin sections, indicated the potential presence of a rare disordered pool of CM in the unit (Marshall et al., 2012; Olcott Marshall et al., 2014; Sforna et al., 2014). Here, in order to refine these findings and to describe the spatial variability in CM structure within the Apex Chert, Raman measurements were conducted on 29 thin sections of samples originating from various locations in the unit. It appears that most of CM in the bedded Apex chert and the hydrothermal dyke exhibit a similar, high degree of maturity, with D1-FWHM between 50 and 65 cm^{-1} (group α samples) corresponding to alteration temperatures of ~ 350 °C (T-D1 geothermometer, Fig. 8-C), consistent with regional greenschist facies metamorphism. There is no evidence of specific hydrothermally-induced graphitization, as documented in e.g. the 2.0 Ga Zaonega formation (Qu et al., 2020). This may be due to differences in organic precursors, differences in hydrothermal conditions (e.g. organic/fluid ratio), or absolute hydrothermal fluid temperatures. However, in group β samples the CM shows a wide range of maturities, corresponding to variations in inferred temperature of a hundred of degrees in a single thin section (Fig. 8-C). Importantly, we found that there is no grouping of individual measurements into distinct pools, i.e. the spectral characteristics vary continuously (Fig. 8-B,C). The location of disordered samples along the outcrop is shown Fig. S5.

We put forward here several hypotheses which may explain these variations:

1) It is known that the degree of thermal alteration in the Pilbara supergroup is - at least locally - controlled by hydrothermal fluid temperature (Harris et al., 2009; Terabayashi et al., 2003). CM of lower maturity could correspond to well-preserved pockets in the Apex chert unit. These relict volumes of the rock were less affected by the circulation of hydrothermal fluids, or only affected by hydrothermal fluids of lower temperature. However, localities where these lower CM maturities are measured correspond mainly to vein cherts and chert breccia, where thermal influence of hydrothermal fluids is expected to be higher than in the layered cherts.

2) CM is in places strongly mixed with small haematite crystals. Haematite has a 1310 cm^{-1} peak in the Raman spectrum that partially overlaps with the D1-peak at 1350 cm^{-1}, leading to anomalously high D-FWHM values of CM. This would lead to an erroneous interpretation of CM maturity, as has been explained by (Marshall et al., 2011). If this is the case, however, other haematite-related peaks should be present in the Raman spectra, which were not observed in our samples. This hypothesis is therefore discarded as an explanation for the disordered CM fraction.

3) Recent weathering by meteoric waters occurred, that either introduced a component of relatively modern biologic contamination or caused disorganization of the structurally ordered CM already present in the rock (Chazhengina and Kovalevski, 2017). This hypothesis is corroborated with the geographic position of the samples containing

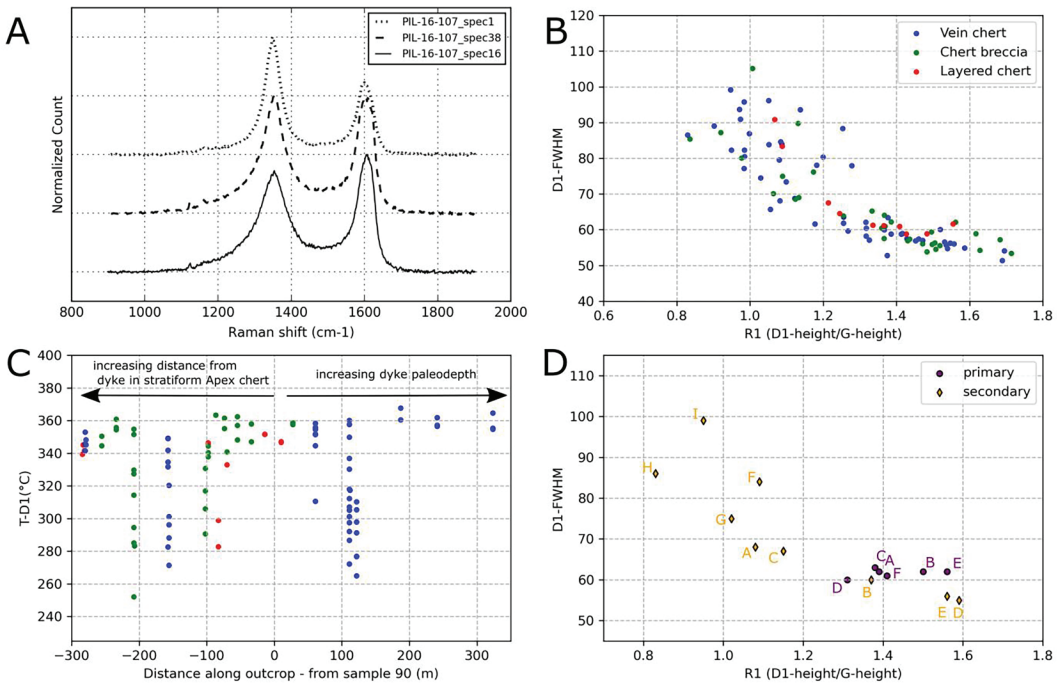

Fig. 8. Raman measurements made on the carbonaceous phases in the Apex chert. **A**: Spectra showing the variability in shape that may be measured in a single thin section (sample PIL-16–107). **B**: comparison of the spectral characteristics for the different spectra. R1 (D1/G peak intensity ratio) plotted against D1-FWHM, obtained using a 5-peak fit for every spectrum measured. Layered chert samples in red, vein chert samples in blue and samples of chert breccia in green. **C**: Temperatures inferred by the T-D1 geothermometer (Kouketsu et al., 2014) for individual spectra according to the position *D* of the sample, using a 5-peak fit for every spectrum. **D**: R1 (D1/G peak intensity ratio) plotted against D1-FWHM for the different spectra obtained on specific primary (purple circles) and secondary (orange diamonds) textures shown in Fig. S4. The labeling of individual spectra corresponds to the labeling of the different pictures in Fig. S4.

disordered organic matter (Fig. S5; Figs. 1 and 8-C); except sample 71, they appear to be located along the banks of the Chinaman Creek river (samples #61,62,65,107,108) or along the banks of its precursor (sample #58). However, the most disordered carbonaceous fractions correspond to temperatures of ca. 240 °C (Fig. 8-C) for the CM, which is incompatible with the direct addition of modern biologic material (although bush fires could also have played a role in altering recent carbonaceous material). Besides, all analyzed CM in our samples is located in areas of the thin sections where no obvious paths (such as cracks) could be observed that would permit the circulation of modern organic material through the chert.

4) Post-metamorphic hydrothermal fluids circulated through the Apex chert, introducing a new, disordered CM component. Such a late-stage disordered component could either represent a specific product of abiotic synthesis associated with hydrothermal processes (Fu et al., 2007; Lollar et al., 2002; Rumble, 2014) or a displaced biologic component from a younger overlying formation. We note that the Apex chert is overlain by pure basalts from the Apex Basalt Formation, and later by the felsic volcanics of the Panorama Formation, which do not contain significant amounts of carbonaceous matter; this favors the scenario of abiotic synthesis during secondary hydrothermal processes. The continuous variation in maturity among the group β samples (no clustering of individual measurement into distinct pools) is an argument against this hypothesis. However, it was observed that the maturity of CM in the organic-rich sedimentary laminations and organic-rich sedimentary clasts shows consistently high maturity (Fig. 8-D and S4, Panel I), while CM that is associated to later void-filling textures, inside botryoids, displays a wide range of maturities (Fig. 8-D and S4, Panel II). These observations suggest that a cooler fluid containing a distinct, less mature pool of organic matter could have circulated in the unit after the main metamorphic event. This fluid locally remobilized more mature, primary CM, which was mixed with the less mature, secondary CM. This mixture of organic matter was then redeposited, notably into the void-filling botryoidal textures found in samples # 61, 107 and 108. If both CM types were mixed in various ratios on a spatial scale smaller than the size of Raman point measurements, this hypothesis could explain the continuous variation in observed maturity. It remains to be explained why only certain samples at specific locations in the stratiform part and the hydrothermal dyke are affected.

Although a more systematic study of the link between texture and maturity would be required to ascertain this scenario, we consider that hypothesis 4) is the most plausible at this stage. As a consequence, if we assume that lower maturities in the unit are probably due to later inputs, then micropaleontologic investigations for syngenetic traces of fossilized life in the Apex should disregard any carbonaceous material with Raman measurements displaying D-widths above ~ 70 cm^{-1} and ID/IG under ~ 1.2.

5.3. *Micropaleontological potential of the Apex chert unit*

5.3.1. *Sedimentary environment*

Fine anisopachous carbonaceous laminations and laminated clasts were found in some samples of the stratiform part (Fig. 3-A,D, and clasts in Fig. 3-E,F). These laminations display irregular oscillations (no fixed wavelength); their formation cannot be explained solely by the action of a laminar flow on fine sedimentary particles. Some laminated clasts also show features of ductile deformation, indicating that the structure was relatively soft when it was remobilized (Fig. 3-E,F). Since these structures are syngenetic with the layered parts of the unit, they could represent microbial biomass that fell from the upper water column (e.g, microbial mats floating on the surface of the water), or microbial mats directly growing on the seafloor substrate. Our study confirms therefore previous findings of similar structures and corroborate the hypothesis of potential biological activity in the surface environments of the Apex chert (Hickman-Lewis et al., 2016). A depletion in light REE correlated with La anomalies (Fig. 9-H) suggests that these Archean communities developed in a basin at least partially open to marine influences. The basin was also affected by continent-derived detrital inputs and volcanic

Table 2
Parameters obtained from Raman spectra measured on carbonaceous fractions in thin sections of different Apex chert samples. *Spectrum*: Number of the sample from which the thin section originates, and number of the Raman spectrum in this thin section. *D*: position of the sample along the outcrop (see Table 1). *Petrology*: type of sample from which the thin section originates; LC: layered chert, VC: vein chert, CB: chert breccia. *D1w*: Full Width at Half Maximum (FWHM) of band D1, obtained with a 5-peak fit, in cm^{-1}. *ID1/IG*: ratio of intensities of peaks D1 and G, obtained using a 5-peak fit. *T-D1*: Geothermometer based on *D1w* (Kouketsu et al., 2014). Note that spectra measured on non-carbonaceous phases or which display low signal-to-noise ratios are not included in this table. For sample 107, a large amount of measurements was made. In order to prevent overrepresentation in the data, only some of the spectra, representing the diversity in maturity among all spectra measured in this thin section, are considered here.

Spectrum	D (m)	petrology	ID1/IG	D1w	T-D1 (°C)
52–6	−283	LC	1,36	61,77	345,19
52–19	−283	LC	1,25	64,51	339,30
52–20	−283	LC	1,39	62	345
52–21	−283	LC	1,50	62	345
52–22	−283	LC	1,38	63	341
53–5	−279	VC	1,18	61,60	345,57
53–6	−279	VC	1,32	58,21	352,85
53–7	−279	VC	1,26	63,51	341,45
54–1	−278	VC	1,26	61,81	345,10
54–4	−278	VC	1,32	60,40	348,14
55–8	−255	CB	1,56	62,10	344,49
55–9	−255	CB	1,50	59,37	350,35
57–1	–233	CB	1,37	57,53	354,32
57–2	–233	CB	1,51	54,52	360,78
57–3	–233	CB	1,43	56,91	355,65
58–2	−207	CB	1,44	57,35	354,69
58–3	−207	CB	1,13	89,74	285,05
58–4-	−207	CB	1,01	105,11	252,00
58–6	−207	CB	1,06	70,09	327,31
58–7	−207	CB	0,88	90,60	283
58–8	−207	CB	0,84	85,36	294,47
58–10	−207	CB	1,62	58,88	351,40
58–12	−207	CB	1,17	76,15	314,28
58–14	−207	CB	1,13	69,00	329,65
61–1	−157	VC	1,08	68,08	331,63
61–2	−157	VC	1,38	63,37	341,75
61–4	−157	VC	1,37	59,93	349,14
61–6	−157	VC	1,52	60,05	348,89
61–7	−157	VC	1,15	67	335
61–8	−157	VC	0,97	90,91	282,54
62–1-	−155	VC	1,08	84,59	296,13
62–2	−155	VC	1,05	96,13	271,31
62–3	−155	VC	1,10	73,38	320,24
62–4-	−155	VC	1,25	88,31	288,13
62–5	−155	VC	0,99	82,27	301,12
65–1	−101	CB	1,12	68,53	330,65
65–2	−101	CB	0,98	80,05	305,90
65–3	−101	CB	1,09	74,95	316,86
66–3	−97	LC	1,34	61,25	346,31
66–4	−97	LC	1,56	61,61	345,55
66–7	−97	LC	1,11	138,57	180,08
68–1	−97	CB	1,33	65,22	337,77
68–2	−97	CB	1,37	64,04	340,32
68–4	−97	CB	1,39	62,18	344,32
71–1	−82	LC	1,07	90,84	282,70
71–2	−82	LC	1,09	83,34	298,82
73–2	−86	CB	1,71	53,36	363,27
75–1	−73	CB	1,63	54,22	361,43
75–2-	−73	CB	1,68	57,19	355,04
76–1	−69	LC	1,21	67,51	332,86
77–2-	−69	CB	1,26	63,85	340,72
80–2-	−54	CB	1,36	60,42	348,11
80–3-	−54	CB	1,51	56,30	356,95
80–6-	−54	CB	1,48	53,80	362,32
87–2-	–33	CB	1,37	60,94	346,97
87–4-	–33	CB	1,50	55,88	357,85
90–1-	−14	LC	1,48	58,87	351,44
90–2-	−14	LC	1,43	58,79	351,61
93–2-	10	LC	1,37	61,13	346,57
93–3-	10	LC	1,41	60,92	347,03
98–1-	27	CB	1,47	56,05	357,50
98–2-	27	CB	1,52	55,55	358,56
102–1	60	VC	1,32	62,07	344,54
102–3	60	VC	1,41	58,77	351,65
102–6	60	VC	1,43	57,46	354,46
102–7	60	VC	1,54	55,72	358,21
104–1	60	VC	1,28	77,91	310,50
104–3	60	VC	1,39	58,79	351,61
104–4	60	VC	1,42	58,92	351,33
104–5	60	VC	1,47	56,98	355,49
104–6	60	VC	1,45	56,89	355,69
107–1	111	VC	1,59	54,87	360,04
107–2	111	VC	1,56	56,02	357,56
107–4	111	VC	1,09	83,98	297,43
107–8	111	VC	1,27	59,64	349,78
107–13	111	VC	1,06	65,69	336,77
107–16	111	VC	0,98	95,75	272,13
107–20	111	VC	1,12	68,75	330,19
107–23	111	VC	1,02	75	317
107–26	111	VC	1,03	74,48	317,87
107–29	111	VC	0,99	80,45	305,03
107–32	111	VC	1,08	79,52	307,03
107–35	111	VC	0,95	82,27	301,13
107–38	111	VC	0,98	77,12	312,18
107–41	111	VC	0,90	89,01	286,62
107–42	111	VC	0,83	86,49	292,05
108–1	121	VC	1,05	83,81	297,81
108–2	121	VC	1,00	86,87	291,22
108–3	121	VC	1,14	93,57	276,83
108–4	121	VC	0,97	93,65	276,65
108–5	121	VC	1,18	78,05	310,19
108–6	121	VC	0,95	99,13	264,86
108–7	121	VC	1,20	80,32	305,32
110–1	187	VC	1,69	51,36	367,58
110–2	187	VC	1,54	54,71	360,37
112–1	241	VC	1,70	54,07	361,75
112–2	241	VC	1,55	56,23	357,11
112–3	241	VC	1,53	56,55	356,42
115–1	323	VC	1,33	57,09	355,26
115–2	323	VC	1,38	52,77	364,55
115–3	323	VC	1,46	57,39	354,61

infalls, evidenced by (i) layers of rounded clasts and angular volcanic shards and (ii) an enrichment in Zr correlated with enrichment in light REE (Fig. 9-D). Dissolved solutes from continentally-derived waters are known to favor primary productivity in modern estuaries and shelf environments (Mallin et al., 1993; Malone et al., 1988). Similar to what has been suggested in the Barberton Greenstone belt (Hickman-Lewis et al., 2020), continental waters (and volcanic infall) may therefore have brought micronutrients and an increased biological activity in this Archean paleoenvironment (Anbar, 2008).

5.3.2. *Extent and intensity of hydrothermal processes in the Apex chert*

The brecciated textures found in the unit are interpreted, similarly to previous reports, to be caused by the injection of multiple pulses of hydrothermal fluids, at least occasionally under phreatic conditions (Brasier et al., 2002, 2005, 2011; Van Kranendonk, 2006). Based on microscopic textural analysis throughout the unit, Brasier et al. (2005), Brasier et al. (2011) reported a strong decrease of hydrothermal influence from the feeder dyke into the stratiform Apex chert. In the current study, however, field observations and microstructural analysis found evidence of hydrothermal influence all along the stratiform Apex chert, with hydro-brecciated cherts sampled as far as 300 to 400 m away from the dyke opening (Figs. 1, 2 and 4). In accordance with our field observations and mapping, we interpret this feature to reflect the emplacement of hydrothermal sills (emanating from the feeder dyke) along the sedimentary layers, causing local cross-cutting and brecciation (Fig. 2). A similar mechanism was documented for the nearby Marble Bar Chert (Van Kranendonk, 2006). The influence of hydrothermal fluids is also supported by REE compositions, with high Eu anomalies

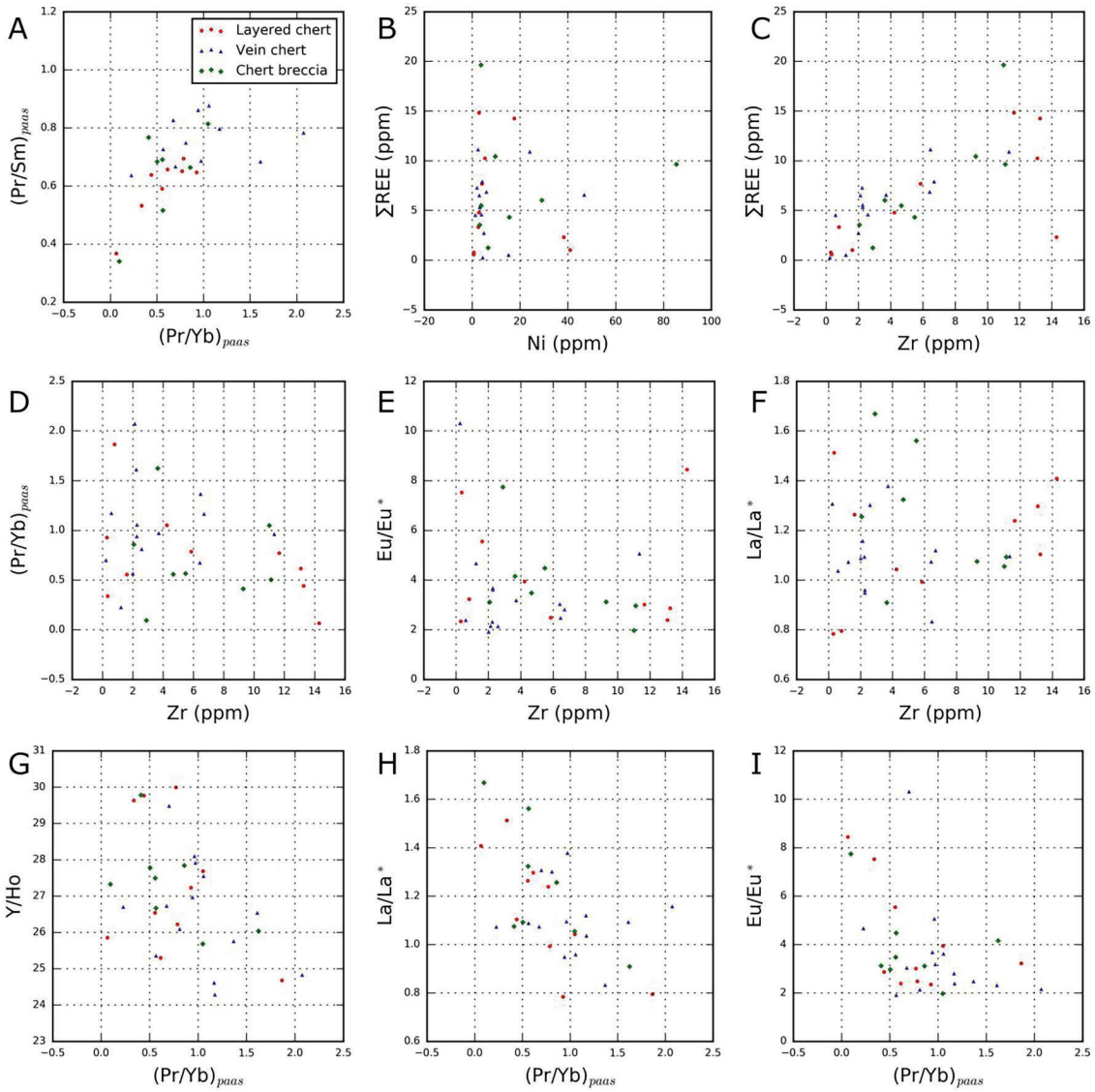

Fig. 9. Plots of pairs of REE–associated parameters calculated for Apex chert samples. Layered chert samples shown as red circles, vein chert samples shown as blue triangles and chert breccia samples shown as green diamonds.

occurring in samples from the dyke to the stratiform part (Fig. 10-A). In general, trace element characteristics do not correlate to the position of samples relatively to the feeder dyke (Fig. 10), which may indicate that the depositional environment did not vary chemically in a systematic fashion from the dyke to the stratiform Apex chert.

The strong brecciation affecting the layered cherts, the presence of cross-cutting veins, and the presence of sills within and along the stratiform part of the unit, all indicate that the most energetic stages of hydrothermal activity took place after initial deposition of the sedimentary precursors of the layered Apex chert. However, Eu anomalies are not correlated with the type of chert considered - samples of layered chert and samples of vein chert display similar Eu anomalies (Table S2). The incorporation of a significant Eu anomaly in samples of sedimentary layered cherts means that hydrothermal fluids circulated in this environment already at the time of deposition of the layered chert precursors. The bottom of the water column was probably mixed with hydrothermal fluids exhaling from nearby vents, and/or hydrothermal fluids were diffusing through unconsolidated sediments. Such a process of diffuse hydrothermal venting was suggested before for cherts in the Barberton Greenstone Belt by Hofmann and Harris, 2008.

5.3.3. Effect of hydrothermal processes on the fossilization, preservation and recognition of life

Modern hydrothermal vents have been found to harbor diverse microbial communities; these communities are based on chemolithotrophic metabolisms that harness the strong redox gradients between hydrothermal fluids and seawater (Brazelton et al., 2006; Jannasch, 1985; Nakagawa et al., 2005; Wang et al., 2009). Many authors believe that hydrothermal environments on the early Earth constituted places where life originated and started to evolve (Deamer and Georgiou, 2015; Martin et al., 2008; Russell et al., 2010; Sojo et al., 2016). As such, the paleoenvironment inferred for the Apex chert unit is an interesting micropaleontological target.

However, hydrothermal environments also greatly complicate the search for unaltered remnants of life and their subsequent interpretation (Buick, 1990):

(1) Hydrothermal fluids and venting systems can favor the formation of abiologic organic molecules - e.g. by Fischer-Tropsch type syntheses (Lollar et al., 2002; McCollom, 2013), and of abiotic structures with life-like morphologies (García-Ruiz et al., 2003;

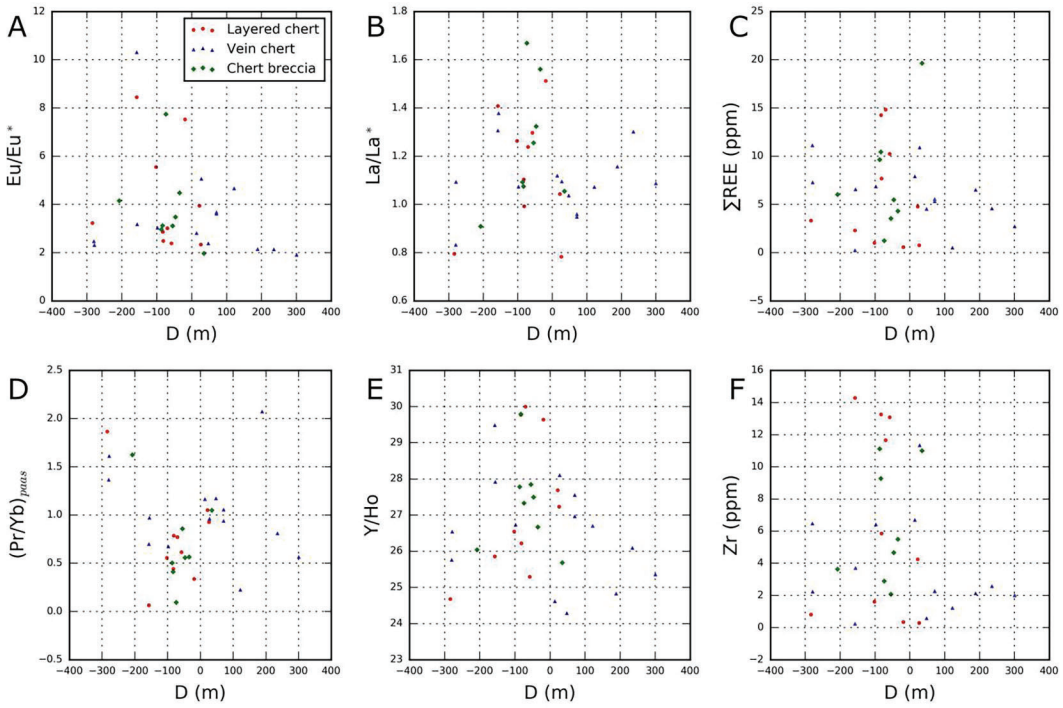

Fig. 10. Relationship between geochemical proxies and position of the samples along the outcrop (see Fig. 1 for correspondence between sample number and sample position). Layered chert samples shown as red circles, vein chert samples shown as blue triangles and chert breccia samples shown as green diamonds.

McMahon, 2019). This obviously complicates the interpretation of organic microstructures found in paleohydrothermal systems.

(2) Hydrothermal fluids accelerate the structural and chemical degradation of biologic structures. This decreases the probability of finding pristine remnants of life in environments with sustained hydrothermal circulation.

(3) Large, dark intrusive cherts indicate a probable advection of carbonaceous materials by hydrothermal fluids in the Apex chert unit. Carbonaceous materials (biologic or not) were probably extensively redistributed within the crust and overlaying sediments (see the "hydrothermal pump" model described by Duda et al., 2018). At smaller scale, diffusion of carbonaceous material may also be observed, for example as dendrites expanding from the organic-rich country rock into the brecciating matrix (Fig. 4-D). Raman measurements in botryoidal textures also indicate that later CM could be mixed at a small spatial scale with primary CM. The displacement of biological structures may prevent an accurate interpretation of their depositional settings and further paleoecological inferences.

The dykes that feed into the Apex chert unit, and where several generations of hydrothermal circulation are observed (Fig. 4-G; Brasier et al., 2011), represent therefore unlikely environments for preserving microbial remnants. Among the roughly 40 thin sections observed from samples collected all along the outcrop, none appeared to contain structures exactly comparable in size and shape to the controversial microfossils reported from the dyke and discussed exhaustively elsewhere (e.g. Bower et al., 2016; Brasier et al., 2005, 2002; Schopf, 1993; Schopf et al., 2018; Schopf and Kudryavtsev, 2009; Schopf and Packer, 1987; Wacey et al., 2015). One round clast in a sample coming from the stratiform part (PIL-16–69) was found to contain elongated carbonaceous structures, but they are branched and are smaller than the structures that were initially described (see Fig. S6). Given the sampling effort, this absence indicates that the structures initially described by Schopf (1987,1993,2002) are extremely rare. The origin of these microstructures is consequently not further discussed here.

Based on petrographic observations and REE patterns, it was established in the current study that hydrothermal circulation has also thoroughly influenced the stratiform part of the unit. Based on the reasons mentioned previously, vein cherts in the stratiform Apex chert should obviously be excluded of paleontological investigation. Critically, evidence of hydrothermal influence was also found in layered cherts, probably due to the mixing of hydrothermal fluids with bottom waters and/or their diffusion through unconsolidated sediments; this urges to caution when interpreting organic microstructures in layered cherts.

Raman measurements indicate the presence of less altered carbonaceous materials in some places of the unit. From textural considerations (see 5.2, Fig. 8-D and Fig. S4), it appears that this CM could originate from the remobilization and mixing of primary CM with a secondary pool of CM during a late hydrothermal circulation event. Interestingly, previous Raman measurements of the controversial microstructures in the dyke (Brasier et al., 2002; Schopf et al., 2002) show them to be constituted of this less altered carbonaceous material.

Overall, the complex depositional environment and diagenetic history leads to strong heterogeneities in the stratiform part of the unit, from the meter to the centimeter scale, which prevent the interpretation of the paleontological potential of a sample solely based on its position relative to main hydrothermal dykes. In this type of geological setting, paleontological discussion requires local evaluation of chemical composition and of organic maturity.

6. Conclusions

The finding of potential microbial mat remnants in the stratiform part of the Apex chert raised questions anew regarding the micropaleontological potential of this unit. We addressed this question here by correlating petrological observations with Trace element compositions and Raman spectroscopic measurements of carbonaceous materials along the unit.

We found carbonaceous laminated structures - with soft deformation features - that may be interpreted as remnants of microbial mats, thus confirming the previous findings of Hickman-Lewis et al. (2016). A

positive linear correlation between REE concentration and Zr concentrations ($r = 0.7$, $p = 2^{*}10^{-6}$) also indicated the significant influence of felsic detrital input in the stratiform part of the unit, and the potential supply of nutrients favoring biological activity into this sedimentary paleoenvironment.

However, a pervasive influence of hydrothermal processes in the stratiform Apex chert was also observed. Petrographic observations in outcrop and in thin section indicate that hydrothermal sills have infiltrated along the sedimentary layers, up to (at least) several hundreds of meters from the main dyke opening; layered cherts were locally veined and brecciated by dense hydrothermal fluids. REE compositions corroborate these observations, with high Eu anomalies (mean Eu/Eu* of 3.83, ranging from 1.91 to 10.32) found as well in layered cherts as in vein cherts, all along the studied outcrop.

This strong hydrothermal influence makes the fine preservation of microfossils in the Apex chert unlikely, and complicates their further paleobiological interpretation. Carbonaceous materials (either biological or abiological) were probably redistributed by hydrothermal fluids in the seafloor crust, following a process similar to the "hydrothermal pump" model described by Duda et al. (2018). Hot hydrothermal fluids would degrade fine biological structures and may also have generated pseudofossils.

Raman geothermometry indicates that, although most of the carbonaceous matter in the unit displays a uniform, high degree of organization (ID/IG of 1.2–1.6, corresponding to inferred peak temperatures around 340 °C), some pockets of a more disordered material (with inferred peak temperatures as low as 200 °C) exist locally in the Apex chert. The presence of a more disordered pool of CM in the unit had been hypothesized in a previous study (Sforna et al., 2014). Here, however, we observe that the maturity of CM in these pockets varies continuously on the centimeter-scale. From textural considerations, the most likely hypothesis is that these pockets represent secondary post-metamorphic inputs mixed with primary, pre-metamorphic CM. The microstructures reported by Schopf (1993), display Raman spectra similar to this more disordered carbonaceous material.

From this discussion, it appears that the probability of finding fine micropaleontological features preserved in the Apex chert is low. Paleontogical exploration of this highly heterogeneous unit also requires petrographic and chemical analyses at multiple spatial scales. As a consequence, we believe that the ratio (expected outcome / required studies) is low for the Apex chert, and that it should not constitute a priority target for Archean micropaleontology. However, the Apex chert unit provides a critical window into the functioning of early hydrothermal systems and their interaction with surface Archean environments.

Declaration of Competing Interest

The authors declare that they have no known competing financial interests or personal relationships that could have appeared to influence the work reported in this paper.

Acknowledgements

We thank the Government of Western Australia (Department of Mines, Industry Regulation and Safety) for its authorization to sample within the State Geoheritage Reserve number R48969. This is IPGP contribution nr. 4242.

Funding information

This comment has received funding from the European Research Council (ERC) under the European Union's Horizon 2020 Research and Innovation Program, Grant Number 646894; and from the Australian Research Council, Centre of Excellence for Core to Crust Fluid Systems.

Appendix A. Supplementary data

Supplementary data to this article can be found online at https://doi.org/10.1016/j.precamres.2021.106415.

References

Alleon, J., Bernard, S., Le Guillou, C., Beyssac, O., Sugitani, K., Robert, F., 2018. Chemical nature of the 3.4 Ga Strelley Pool microfossils. Geochem. Perspect. Lett. 37–42 https://doi.org/10.7185/geochemlet.1817.

Alleon, J., Bernard, S., Le Guillou, C., Daval, D., Skouri-Panet, F., Pont, S., Delbes, L., Robert, F., 2016. Early entombment within silica minimizes the molecular degradation of microorganisms during advanced diagenesis. Chem. Geol. 437, 98–108. https://doi.org/10.1016/j.chemgeo.2016.05.034.

Allwood, A.C., Kamber, B.S., Walter, M.R., Burch, I.W., Kanik, I., 2010. Trace elements record depositional history of an Early Archean stromatolitic carbonate platform. Chem. Geol. 270, 148–163. https://doi.org/10.1016/j.chemgeo.2009.11.013.

Anbar, A.D., 2008. Elements and Evolution. Science 322, 1481–1483.

Aoya, M., Kouketsu, Y., Endo, S., Shimizu, H., Mizukami, T., Nakamura, D., Wallis, S., 2010. Extending the applicability of the Raman carbonaceous-material geothermometer using data from contact metamorphic rocks: RAMAN CARBONACEOUS-MATERIAL GEOTHERMOMETER. J. Metamorph. Geol. 28, 895–914. https://doi.org/10.1111/j.1525-1314.2010.00896.x.

Arndt, N.T., Nisbet, E.G., 2012. Processes on the Young Earth and the Habitats of Early Life. Annu. Rev. Earth Planet. Sci. 40, 521–549. https://doi.org/10.1146/annurev-earth-042711-105316.

Barghoorn, E.S., Tyler, S.A., 1965. Microorganisms from the Gunflint Chert. Sci. New Ser. 147, 563–577.

Bau, M., Dulski, P., 1999. Comparing yttrium and rare earths in hydrothermal fluids from the Mid-Atlantic Ridge: implications for Y and REE behaviour during near-vent mixing and for the YrHo ratio of Proterozoic seawater 14.

Bau, M., Dulski, P., 1996. Distribution of yttrium and rare-earth elements in the Penge and Kuruman iron-formations, Transvaal Supergroup. South Africa. Precambrian Res. 79, 37–55. https://doi.org/10.1016/0301-9268(95)00087-9.

Beyssac, O., Goffé, B., Chopin, C., Rouzaud, J.-N., 2002. Raman spectra of carbonaceous material in metasediments: a new geothermometer. J. Metamorph. Geol. 20, 859–871.

Bolhar, R., Kamber, B.S., Moorbath, S., Fedo, C.M., Whitehouse, M.J., 2004. Characterisation of early Archaean chemical sediments by trace element signatures. Earth Planet. Sci. Lett. 222, 43–60. https://doi.org/10.1016/j.epsl.2004.02.016.

Bolhar, R., Kamber, B.S., Moorbath, S., Whitehouse, M.J., Collerson, K.D., 2005. Chemical characterization of earth's most ancient clastic metasediments from the Isua Greenstone Belt, southern West Greenland. Geochimica et Cosmochimica Acta 69, 1555–1573.

Bolhar, R., Van Kranendonk, M.J., Kamber, B.S., 2005. A trace element study of siderite–jasper banded iron formation in the 3.45Ga Warrawoona Group, Pilbara Craton—Formation from hydrothermal fluids and shallow seawater. Precambrian Res. 137, 93–114. https://doi.org/10.1016/j.precamres.2005.02.001.

Bolhar, R., Vankranendonk, M., 2007. A non-marine depositional setting for the northern Fortescue Group, Pilbara Craton, inferred from trace element geochemistry of stromatolitic carbonates. Precambrian Res. 155, 229–250. https://doi.org/10.1016/j.precamres.2007.02.002.

Bolhar, R., Hofmann, A., Siahi, M., Feng, Y.-X., Delvigne, C., 2015. A trace element and Pb isotopic investigation into the provenance and deposition of stromatolitic carbonates, ironstones and associated shales of the ~3.0 Ga Pongola Supergroup. Kaapvaal Craton. Geochim. Cosmochim. Acta 158, 57–78.

Bower, D.M., Steele, A., Fries, M.D., Green, O.R., Lindsay, J.F., 2016. Raman Imaging Spectroscopy of a Putative microfossil from the 3.46 Ga Apex chert: Insights from Quartz Grain Orientation. Astrobiology 16, 169–180. https://doi.org/10.1089/ast.2014.1207.

Brasier, M.D., Green, O.R., Jephcoat, A.P., Kleppe, A.K., Van Kranendonk, M.J., Lindsay, J.F., Steele, A., Grassineau, N.V., 2002. Questioning the evidence for Earth's oldest fossils. Nature 416, 76–81. https://doi.org/10.1038/416076a.

Brasier, M.D., Green, O.R., Lindsay, J.F., Mcloughlin, N., Steele, A., Stoakes, C., 2005. Critical testing of Earth's oldest putative fossil assemblage from the ~3. 5 Ga Apex chert, Chinaman Creek. Western Australia. Precambrian Res. 140, 55–102. https://doi.org/10.1016/j.precamres.2005.06.008.

Brasier, M.D., Green, O.R., Lindsay, J.F., McLoughlin, N., Stoakes, C.A., Brasier, A.T., Wacey, D., 2011. Geology and putative microfossil assemblage of the ca. 3460 Ma "Apex Chert". Western Australia - A field and petrographic guide. Geological Survey of Western Australia, Perth.

Brazelton, W.J., Schrenk, M.O., Kelley, D.S., Baross, J.A., 2006. Methane- and Sulfur-Metabolizing Microbial Communities Dominate the Lost City Hydrothermal Field Ecosystem. Appl. Environ. Microbiol. 72, 6257–6270. https://doi.org/10.1128/AEM.00574-06.

Buick, R., 1990. Microfossil Recognition in Archean Rocks: An Appraisal of Spheroids and Filaments from a 3500 M.Y. Old Chert-Barite Unit at North Pole. Western Australia. Palaios 5, 441–459.

Bustin, R.M., Rouzaud, J.N., Ross, J.V., 1995. Natural graphitization of anthracite: Experimental considerations. Carbon 33, 679–691. https://doi.org/10.1016/0008-6223(94)00155-S.

Chazhengina, S.Y., Kovalevski, V.V., 2017. Raman spectroscopy of weathered shungites: Raman spectroscopy of weathered shungites. J. Raman Spectrosc. 48, 1590–1596. https://doi.org/10.1002/jrs.5188.

Condie, K.C., 1993. Chemical composition and evolution of the upper continental crust: Contrasting results from surface samples and shales. Chem. Geol. 104, 1–37. https://doi.org/10.1016/0009-2541(93)90140-E.

Danielson, A., Möller, P., Dulski, P., 1992. The europium anomalies in banded iron formations and the thermal history of the oceanic crust. Chem. Geol. 97, 89–100. https://doi.org/10.1016/0009-2541(92)90137-T.

De Gregorio, B.T., Sharp, T.G., Rushdi, A.I., Simoneit, B.R.T., 2010. Bugs or Gunk ? Nanoscale Methods for Assessing the Biogenicity of Ancient Microfossils and Organic Matter. https://doi.org/10.1007/978-90-481-8794-2.

Deamer, D.W., Georgiou, C.D., 2015. Hydrothermal Conditions and the Origin of Cellular Life. Astrobiology 15, 1091–1095. https://doi.org/10.1089/ast.2015.1338.

Delarue, F., Rouzaud, J.-N., Derenne, S., Bourbin, M., Westall, F., Kremer, B., Sugitani, K., Deldicque, D., Robert, F., 2016. The Raman-Derived Carbonization Continuum: A Tool to Select the Best Preserved Molecular Structures in Archean Kerogens. Astrobiology 16, ast.2015.1392. 10.1089/ast.2015.1392.

Douville, E., Charlou, J.L., Oelkers, E.H., Bienvenu, P., Colon, C.J., Donval, J.P., Fouquet, Y., Prieur, D., Appriou, P., 2002. The rainbow vent fluids (36 14′ N, MAR): the influence of ultramafic rocks and phase separation on trace metal content in Mid-Atlantic Ridge hydrothermal fluids. Chem. Geol. 184, 37–48.

Duda, J.-P., Thiel, V., Bauersachs, T., Mißbach, H., Reinhardt, M., Schäfer, N., Van Kranendonk, M.J., Reitner, J., 2018. Ideas and perspectives: hydrothermally driven redistribution and sequestration of early Archaean biomass – the "hydrothermal pump hypothesis". Biogeosciences 15, 1535–1548. https://doi.org/10.5194/bg-15-1535-2018.

Elderfield, H., Upstill-Goddard, R., Sholkovitz, E.R., 1990. The rare earth elements in rivers, estuaries, and coastal seas and their significance to the composition of ocean waters. Geochim. Cosmochim. Acta 54, 971–991. https://doi.org/10.1016/0016-7037(90)90432-K.

Fu, Q., Sherwood Lollar, B., Horita, J., Lacrampe-Couloume, G., Seyfried, W.E., 2007. Abiotic formation of hydrocarbons under hydrothermal conditions: Constraints from chemical and isotope data. Geochim. Cosmochim. Acta 71, 1982–1998. https://doi.org/10.1016/j.gca.2007.01.022.

García-Ruiz, J.M., Hyde, S.T., Carnerup, M., Christy, G., Kranendonk, M.J.V., Welham, N. J., 2003. Self-assembled Silica-Carbonate Structures and Detection of Ancient microfossils. Science 302, 1194–1197. https://doi.org/10.1126/science.1090163.

García-Ruiz, J.M., van Zuilen, M., Bach, W., 2020. Mineral self-organization on a lifeless planet. Phys. Life Rev. S1571064520300014 https://doi.org/10.1016/j.plrev.2020.01.001.

Gourcerol, B., Thurston, P.C., Kontak, D.J., Côté-Mantha, O., 2015. Interpretations and implications of LA ICP-MS analysis of chert for the origin of geochemical signatures in banded iron formations (BIFs) from the Meadowbank gold deposit, Western Churchill Province. Nunavut. Chem. Geol. 410, 89–107. https://doi.org/10.1016/j.chemgeo.2015.06.008.

Harris, A.C., White, N.C., McPhie, J., Bull, S.W., Line, M.A., Skrzeczynski, R., Mernagh, T. P., Tosdal, R.M., 2009. Early Archean Hot Springs above Epithermal Veins, North Pole, Western Australia: New Insights from Fluid Inclusion Microanalysis. Econ. Geol. 104, 793–814. https://doi.org/10.2113/gsecongeo.104.6.793.

Hickman-Lewis, K., Cavalazzi, B., Foucher, F., Westall, F., 2018. Most ancient evidence for life in the Barberton greenstone belt: Microbial mats and biofabrics of the ~3.47 Ga Middle Marker horizon. Precambrian Res. 312, 45–67. https://doi.org/10.1016/j.precamres.2018.04.007.

Hickman-Lewis, K., Garwood, R.J., Brasier, M.D., Goral, T., Jiang, H., McLoughlin, N., Wacey, D., 2016. Carbonaceous microstructures from sedimentary laminated chert within the 3.46Ga Apex Basalt, Chinaman Creek locality, Pilbara. Western Australia. Precambrian Res. 278, 161–178. https://doi.org/10.1016/j.precamres.2016.03.013.

Hickman-Lewis, K., Gourcerol, B., Westall, F., Manzini, D., Cavalazzi, B., 2020. Reconstructing Palaeoarchaean microbial biomes flourishing in the presence of emergent landmasses using trace and rare earth element systematics. Precambrian Res. 342, 105689 https://doi.org/10.1016/j.precamres.2020.105689.

Hofmann, A., Harris, C., 2008. Silica alteration zones in the Barberton greenstone belt: A window into subseafloor processes 3.5–3.3 Ga ago. Chem. Geol. 257, 221–239. https://doi.org/10.1016/j.chemgeo.2008.09.015.

Jannasch, H.W., 1985. Review Lecture - The chemosynthetic support of life and the microbial diversity at deep-sea hydrothermal vents. Proc. R. Soc. Lond. B Biol. Sci. 225, 277–297. https://doi.org/10.1098/rspb.1985.0062.

Kamber, B.S., Bolhar, R., Webb, G.E., 2004. Geochemistry of late Archaean stromatolites from Zimbabwe: evidence for microbial life in restricted epicontinental seas. Precambrian Res. 132, 379–399. https://doi.org/10.1016/j.precamres.2004.03.006.

Kamber, B.S., Webb, G.E., 2001. The geochemistry of late Archaean microbial carbonate: implications for ocean chemistry and continental erosion history. Geochim. Cosmochim. Acta 65, 2509–2525. https://doi.org/10.1016/S0016-7037(01)00613-5.

Kamber, B.S., Webb, G.E., Gallagher, M., 2014. The rare earth element signal in Archaean microbial carbonate: information on ocean redox and biogenicity. J. Geol. Soc. 171, 745–763. https://doi.org/10.1144/jgs2013-110.

Kato, Y., Nakamura, K., 2003. Origin and global tectonic significance of Early Archean cherts from the Marble Bar greenstone belt, Pilbara Craton. Western Australia. Precambrian Res. 125, 191–243. https://doi.org/10.1016/S0301-9268(03)00043-3.

Konhauser, K., 2007. Introduction to geomicrobiology. Blackwell Publishing.

Kouketsu, Y., Mizukami, T., Mori, H., Endo, S., Aoya, M., Hara, H., Nakamura, D., Wallis, S., 2014. A new approach to develop the Raman carbonaceous material geothermometer for low-grade metamorphism using peak width. Isl. Arc 23, 33–50. https://doi.org/10.1111/iar.12057.

Lahfid, A., Beyssac, O., Deville, E., Negro, F., Chopin, C., Goffe, B., 2010. Evolution of the Raman spectrum of carbonaceous material in low-grade metasediments of the Glarus Alps (Switzerland). Terra Nova 1–7. https://doi.org/10.1111/j.1365-3121.2010.00956.x.

Ledevin, M., Arndt, N., Simionovici, A., Jaillard, E., Ulrich, M., 2014. Silica precipitation triggered by clastic sedimentation in the Archean: New petrographic evidence from cherts of the Kromberg type section. South Africa. Precambrian Res. 255, 316–334. https://doi.org/10.1016/j.precamres.2014.10.009.

Lollar, B.S., Westgate, T.D., Ward, J.A., Slater, G.F., Lacrampe-Couloume, G., 2002. Abiogenic formation of alkanes in the Earth's crust as a minor source for global hydrocarbon reservoirs. Nature 416, 3.

Mallin, M.A., Paerl, H.W., Rudek, J., Bates, P.W., 1993. Regulation of estuarine primary production by watershed rainfall and river flow. Mar. Ecol. Prog. Ser. 93, 199–203. https://doi.org/10.3354/meps093199.

Malone, T.C., Crocker, L.H., Pike, S.E., Wendler, B.W., 1988. Influences of river flow on the dynamics of phytoplankton production in a partially stratified estuary. Mar. Ecol. Prog. Ser. 48, 235–249. https://doi.org/10.3354/meps048235.

Marshall, A.O., Emry, J.R., Marshall, C.P., 2012. Multiple Generations of Carbon in the Apex Chert and Implications for Preservation of Microfossils. Astrobiology 12, 160–166. https://doi.org/10.1089/ast.2011.0729.

Marshall, C.P., Emry, J.R., Marshall, A.O., 2011. Haematite pseudomicrofossils present in the 3. 5-billion-year-old Apex Chert. Nat. Geosci. 4, 240–243. https://doi.org/10.1038/NGEO1084.

Martin, W., Baross, J., Kelley, D., Russell, M.J., 2008. Hydrothermal vents and the origin of life. Nat. Rev. Microbiol. 6, 805–814. https://doi.org/10.1038/nrmicro1991.

McCollom, T.M., 2013. Laboratory Simulations of Abiotic Hydrocarbon Formation in Earth's Deep Subsurface. Rev. Mineral. Geochem. 75, 467–494. https://doi.org/10.2138/rmg.2013.75.15.

McCollom, T.M., Seewald, J.S., 2006. Carbon isotope composition of organic compounds produced by abiotic synthesis under hydrothermal conditions. Earth Planet. Sci. Lett. 243, 74–84. https://doi.org/10.1016/j.epsl.2006.01.027.

McMahon, S., 2019. Earth's earliest and deepest purported fossils may be iron-mineralized chemical gardens. Proc. R. Soc. B Biol. Sci. 286, 20192410. https://doi.org/10.1098/rspb.2019.2410.

Milesi, V., Guyot, F., Brunet, F., Richard, L., Recham, N., Benedetti, M., Dairou, J., Prinzhofer, A., 2015. Formation of CO2, H2 and condensed carbon from siderite dissolution in the 200–300°C range and at 50MPa. Geochim. Cosmochim. Acta 154, 201–211. https://doi.org/10.1016/j.gca.2015.01.015.

Mitra, A., Elderfield, H., Greaves, M.J., 1994. Rare earth elements in submarine hydrothermal fluids and plumes from the Mid-Atlantic Ridge. Mar. Chem. 46, 217–235. https://doi.org/10.1016/0304-4203(94)90079-5.

Nakagawa, S., Takai, K., Inagaki, F., Chiba, H., Ishibashi, J., Kataoka, S., Hirayama, H., Nunoura, T., Horikoshi, K., Sako, Y., 2005. Variability in microbial community and venting chemistry in a sediment-hosted backarc hydrothermal system: Impacts of subseafloor phase-separation. FEMS Microbiol. Ecol. 54, 141–155. https://doi.org/10.1016/j.femsec.2005.03.007.

Noffke, N., Christian, D., Wacey, D., Hazen, R.M., 2013. Microbially Induced Sedimentary Structures Recording an Ancient Ecosystem in the *ca.* 3.48 Billion-Year-Old Dresser Formation, Pilbara. Western Australia. Astrobiology 13, 1103–1124. https://doi.org/10.1089/ast.2013.1030.

Nozaki, Y., Zhang, J., Amakawa, H., 1997. The fractionation between Y and Ho in the marine environment. Earth Planet. Sci. Lett. 148, 329–340. https://doi.org/10.1016/S0012-821X(97)00034-4.

Oehler, J.H., 1976. Experimental studies in Precambrian paleontology: Structural and chemical changes in blue-green algae during simulated fossilization in synthetic chert. Bull. Geol. Soc. Am. 87, 117–129. https://doi.org/10.1130/0016-7606(1976)87<117:ESIPPS>2.0.CO;2.

Olcott Marshall, A., Jehlička, J., Rouzaud, J.-N., Marshall, C.P., 2014. Multiple generations of carbonaceous material deposited in Apex chert by basin-scale pervasive hydrothermal fluid flow. Gondwana Res. 25, 284–289. https://doi.org/10.1016/j.gr.2013.04.006.

Pasteris, J.D., Wopenka, B., 2003. Necessary, but Not Sufficient: Raman Identification of Disordered Carbon as a Signature of Ancient Life. Astrobiology 3.

Pinti, D.L., Mineau, R., Clement, V., 2009. Hydrothermal alteration and microfossil artefacts of the 3,465-million-year-old Apex chert. Nat. Geosci. 2, 640–643. https://doi.org/10.1038/ngeo601.

Preston, L.J., Genge, M.J., 2010. The Rhynie Chert, Scotland, and the search for life on Mars. Astrobiology 10, 549–560. https://doi.org/10.1089/ast.2008.0321.

Qu, Y., Engdahl, A., Zhu, S., Vajda, V., McLoughlin, N., 2015. Ultrastructural Heterogeneity of Carbonaceous Material in Ancient Cherts : Investigating Biosignature Origin and Preservation. Astrobiology 15, 825–842. https://doi.org/10.1089/ast.2015.1298.

Qu, Y., van Zuilen, M.A., Lepland, A., 2020. Hydrothermal circulation and oil migration at the root of the heterogeneous micro-structure of carbonaceous material in the 2.0 Ga Zaonega Formation, Onega Basin, Russia. Precambrian Res. 105705 https://doi.org/10.1016/j.precamres.2020.105705.

Rouchon, V., Orberger, B., 2008. Origin and mechanisms of K-Si-metasomatism of ca. 3.4–3.3Ga volcaniclastic deposits and implications for Archean seawater evolution: Examples from cherts of Kittys Gap (Pilbara craton, Australia) and Msauli (Barberton Greenstone Belt, South Africa). Precambrian Res. 165, 169–189. https://doi.org/10.1016/j.precamres.2008.06.003.

Rouillard, J., García-Ruiz, J.-M., Gong, J., van Zuilen, M.A., 2018. A morphogram for silica-witherite biomorphs and its application to microfossil identification in the early earth rock record. Geobiology 16, 279–296. https://doi.org/10.1111/gbi.12278.

Rouzaud, J.-N., Deldicque, D., Charon, E., Pageot, J., 2015. Carbons at the heart of questions on energy and environment : A nanostructural approach. Comptes Rendus Geosci. 347, 124–133. https://doi.org/10.1016/j.crte.2015.04.004.

Rudnick, R.L., 2003. 3.01 - Composition of the Continental Crust. In: Treatise on Geochemistry. Elsevier Ltd, p. 64.
Rumble, D., 2014. Hydrothermal Graphitic Carbon. Elements 10, 427–433. https://doi.org/10.2113/gselements.10.6.427.
Russell, M.J., Hall, A.J., Martin, W., 2010. Serpentinization as a source of energy at the origin of life: Serpentinization and the emergence of life. Geobiology 8, 355–371. https://doi.org/10.1111/j.1472-4669.2010.00249.x.
Schopf, J.W., 2007. Earliest evidence of life on earth. Precambrian Res. 158, 139–140. https://doi.org/10.1016/j.precamres.2007.05.001.
Schopf, J.W., 1993. Microfossils of the Early Archean Apex Chert: New Evidence of the Antiquity of Life. Sci. New Ser. 260, 640–646.
Schopf, J.W., Kitajima, K., Spicuzza, M.J., Kudryavtsev, A.B., Valley, J.W., 2018. SIMS analyses of the oldest known assemblage of microfossils document their taxon-correlated carbon isotope compositions. Proc. Natl. Acad. Sci. 115, 53–58. https://doi.org/10.1073/pnas.1718063115.
Schopf, J.W., Kudryavtsev, A.B., 2009. Confocal laser scanning microscopy and Raman imagery of ancient microscopic fossils. Precambrian Res. 173, 39–49. https://doi.org/10.1016/j.precamres.2009.02.007.
Schopf, J.W., Kudryavtsev, A.B., Agresti, D.G., Wdowiak, T.J., Czaja, A.D., 2002. Laser-Raman imagery of Earth's earliest fossils. Nature 416, 73–76.
Schopf, J.W., Packer, B., 1987. Early Archean (3.3-billion to 3.5-billion-year-old) microfossils from Warrawoona Group. Australia. Science 237, 70–73. https://doi.org/10.1126/science.11539686.
Sforna, M.C., van Zuilen, M.A., Philippot, P., 2014. Structural characterization by Raman hyperspectral mapping of organic carbon in the 3.46 billion-year-old Apex chert. Western Australia. Geochim. Cosmochim. Acta 124, 18–33. https://doi.org/10.1016/j.gca.2013.09.031.
Sholkovitz, E.R., Landing, W.M., Lewis, B.L., 1994. Ocean particle chemistry: The fractionation of rare earth elements between suspended particles and seawater. Geochim. Cosmochim. Acta 58, 1567–1579. https://doi.org/10.1016/0016-7037(94)90559-2.
Siever, R., 1992. The silica cycle in the Precambrian. Geochimica et Cosmochimica Acta 56, 3265–3272.
Sojo, V., Herschy, B., Whicher, A., Camprubí, E., Lane, N., 2016. The Origin of Life in Alkaline Hydrothermal Vents. Astrobiology 16, 181–197. https://doi.org/10.1089/ast.2015.1406.
Sugahara, H., Sugitani, K., Mimura, K., Yamashita, F., Yamamoto, K., 2010. A systematic rare-earth elements and yttrium study of Archean cherts at the Mount Goldsworthy greenstone belt in the Pilbara Craton: Implications for the origin of microfossil-bearing black cherts. Precambrian Res. 177, 73–87. https://doi.org/10.1016/j.precamres.2009.10.005.
Sugitani, K., Grey, K., Nagaoka, T., Mimura, K., Walter, M.R., 2009. Taxonomy and biogenicity of Archaean spheroidal microfossils (ca. 3.0 Ga) from the Mount Goldsworthy-Mount Grant area in the northeastern Pilbara Craton. Western Australia. Precambrian Res. 173, 50–59. https://doi.org/10.1016/j.precamres.2009.02.004.
Sugitani, K., Nagaoka, T., Mimura, K., Grey, K., Kranendonk, M.V., 2006. Discovery of possible microfossils from c . 3 . 4 Ga Strelley Pool Chert , Kelly Group , Pilbara Craton : evidence for antiquity of life and biotic diversity ?, in: Geoscience Research Abstracts. Presented at the European Geosciences Union 2006.
Takahashi, Y., Châtellier, X., Hattori, K.H., Kato, K., Fortin, D., 2005. Adsorption of rare earth elements onto bacterial cell walls and its implication for REE sorption onto natural microbial mats. Chem. Geol. 219, 53–67. https://doi.org/10.1016/j.chemgeo.2005.02.009.
Terabayashi, M., Masada, Y., Ozawa, H., 2003. Archean ocean-floor metamorphism in the North Pole area, Pilbara Craton. Western Australia. Precambrian Res. 127, 167–180. https://doi.org/10.1016/S0301-9268(03)00186-4.
Thiry, M., Milnes, A.R., Rayot, V., Simon-CoinÇon, R., 2006. Interpretation of palaeoweathering features and successive silicifications in the Tertiary regolith of inland Australia. J. Geol. Soc. 163, 723–736. https://doi.org/10.1144/0014-764905-020.
Thurston, P.C., Kamber, B.S., Whitehouse, M., 2012. Archean cherts in banded iron formation: Insight into Neoarchean ocean chemistry and depositional processes. Precambrian Res. 214–215, 227–257. https://doi.org/10.1016/j.precamres.2012.04.004.
Tice, M.M., Lowe, D.R., 2006. The origin of carbonaceous matter in pre-3.0 Ga greenstone terrains: A review and new evidence from the 3.42 Ga Buck Reef Chert. Earth-Sci. Rev. 76, 259–300. https://doi.org/10.1016/j.earscirev.2006.03.003.
Trower, E.J., Lowe, D.R., 2016. Sedimentology of the ~3.3 Ga upper Mendon Formation, Barberton Greenstone Belt. South Africa. Precambrian Res. 281, 473–494. https://doi.org/10.1016/j.precamres.2016.06.003.
van den Boorn, S.H.J.M., Van Bergen, M.J., Nijman, W., Vroon, P.Z., 2007. Dual role of seawater and hydrothermal fluids in Early Archean chert formation: Evidence from silicon isotopes. Geology 35, 939–942. https://doi.org/10.1130/G24096A.1.
van den Boorn, S.H.J.M., van Bergen, M.J., Vroon, P.Z., de Vries, S.T., Nijman, W., 2010. Silicon isotope and trace element constraints on the origin of ~3.5Ga cherts: Implications for Early Archaean marine environments. Geochim. Cosmochim. Acta 74, 1077–1103. https://doi.org/10.1016/j.gca.2009.09.009.
Van Kranendonk, M.J., 2006. Volcanic degassing, hydrothermal circulation and the flourishing of early life on Earth: A review of the evidence from c. 3490–3240 Ma rocks of the Pilbara Supergroup, Pilbara Craton. Western Australia. Earth-Sci. Rev. 74, 197–240. https://doi.org/10.1016/j.earscirev.2005.09.005.
Van Kranendonk, M.J., Hugh Smithies, R., Hickman, A.H., Champion, D.C., 2007. Review: secular tectonic evolution of Archean continental crust: interplay between horizontal and vertical processes in the formation of the Pilbara Craton, Australia. Terra Nova 19, 1–38. https://doi.org/10.1111/j.1365-3121.2006.00723.x.
Van Kranendonk, M.J., Pirajno, F., 2004. Geochemistry of metabasalts and hydrothermal alteration zones associated with c. 3.45 Ga chert and barite deposits: implications for the geological setting of the Warrawoona Group, Pilbara Craton. Australia. Geochem. Explor. Environ. Anal. 4, 253–278. https://doi.org/10.1144/1467-7873/04-205.
Van Kranendonk, M.J., Webb, G.E., Kamber, B.S., 2003. Geological and trace element evidence for a marine sedimentary environment of deposition and biogenicity of 3.45 stromatolitic carbonates in the Pilbara Craton, in support for a reducing Archean ocean. Geobiology 1, 91–108.
van Zuilen, M.A., Fliegel, D., Wirth, R., Lepland, A., Qu, Y., Schreiber, A., Romashkin, A. E., Philippot, P., 2012. Mineral-templated growth of natural graphite films. Geochim. Cosmochim. Acta 83, 252–262. https://doi.org/10.1016/j.gca.2011.12.030.
Wacey, D., Saunders, M., Kong, C., Brasier, A., Brasier, M., 2015. 3.46 Ga Apex chert "microfossils" reinterpreted as mineral artefacts produced during phyllosilicate exfoliation. Gondwana Res. 36, 296–313. https://doi.org/10.1016/j.gr.2015.07.010.
Wang, F., Zhou, H., Meng, J., Peng, X., Jiang, L., Sun, P., Zhang, C., Van Nostrand, J.D., Deng, Y., He, Z., Wu, L., Zhou, J., Xiao, X., 2009. GeoChip-based analysis of metabolic diversity of microbial communities at the Juan de Fuca Ridge hydrothermal vent. Proc. Natl. Acad. Sci. 106, 4840–4845. https://doi.org/10.1073/pnas.0810418106.
Westall, F., Cavalazzi, B., Lemelle, L., Marrocchi, Y., Rouzaud, J.-N., Simionovici, A., Salomé, M., Mostefaoui, S., Andreazza, C., Foucher, F., Toporski, J., Jauss, A., Thiel, V., Southam, G., MacLean, L., Wirick, S., Hofmann, A., Meibom, A., Robert, F., Défarge, C., 2011. Implications of in situ calcification for photosynthesis in a ~3.3Ga-old microbial biofilm from the Barberton greenstone belt. South Africa. Earth Planet. Sci. Lett. 310, 468–479. https://doi.org/10.1016/j.epsl.2011.08.029.
Wheat, C.G., Mottl, M.J., Rudnicki, M., 2002. Trace element and REE composition of a low-temperature ridge-flank hydrothermal spring. Geochim. Cosmochim. Acta 66, 3693–3705. https://doi.org/10.1016/S0016-7037(02)00894-3.